Defence Research and Development Canada
Recherche et développement pour la défense Canada

DEFENCE R&D DÉFENSE

Change detection using RADARSAT-1 interferometry: Mine site monitoring

Karim E. Mattar

Defence R&D Canada – Ottawa
TECHNICAL MEMORANDUM
DRDC Ottawa TM 2004-261
December 2004

Canada

Change detection using RADARSAT-1 interferometry: mine site monitoring

Karim E. Mattar
DRDC Ottawa

Defence R&D Canada – Ottawa

Technical Memorandum

DRDC Ottawa TM 2004-261

December 2004

Abstract

This study examines the potential of using satellite repeat-pass interferometry for wide-area surveillance and change detection. Several RADARSAT-1 interferometric datasets were acquired in 2003 over active mines in South Australia and Saskatchewan, Canada. Three-colour RGB images derived from the various image magnitudes supplements and complements the interferometric coherence information for detecting even subtle scene changes. Together they were found to be a potentially valuable tool for wide area surveillance and long term site monitoring, providing potentially important contextual information. The limited resolution of RADARSAT-1 did not permit conclusive assessment of changes detectable in the mine complex itself, and the lack of ground truth did not permit accurate terrain height estimation. The absence of ring-like phase patterns that characterize decimetre-level terrain subsidence implies that terrain subsidence was not present within the scene.

Résumé

La présente étude examine la possibilité d'utiliser l'interférométrie par satellite à passage répété pour la surveillance de surfaces étendues et la détection de changements. Plusieurs ensembles de données interférométriques RADARSAT-1 ont été obtenus en 2003 sur des mines actives en Australie-Méridionale et en Saskatchewan au Canada. Des images RVB trois couleurs dérivées de diverses magnitudes d'images complètent les renseignements de cohérence interférométrique et permettent de détecter les changements de scène, même les plus faibles. Ensemble, ces images se sont révélées un outil éventuellement précieux pour la surveillance de surfaces étendues et l'observation de sites à long terme avec la promesse de renseignements contextuels importants. La résolution limitée de RADARSAT-1 a empêché une évaluation concluante des changements discernables dans le complexe minier, et l'absence de réalité de terrain n'a pas permis l'estimation précise de la hauteur du terrain. L'absence de motifs de phase en anneaux, une caractéristique de subsidence mesurable en décimètres, suggère qu'il n'y avait pas de subsidence dans la scène.

This page intentionally left blank.

Executive summary

This report concludes a study examining the potential application of satellite repeat-pass interferometry (SRI) for change detection. The goal of the project is to develop tools for wide area surveillance and monitoring of mines.

This project was partially supported by, and was carried out in collaboration with, the Canadian Nuclear Safety Commission (CNSC). They are interested in imagery and tools that would permit remote monitoring of uranium mines for the purpose of assessing compliance with international treaties. Two active uranium mines were chosen as the sites for this study. They include Range Mine in South Australia and Key Lakes Mine in Saskatchewan, Canada. These sites were chosen, at the suggestion of CNSC, because corroborative evidence could potentially be obtained. They were also sites of previous studies supported by CNSC.

Several sets of RADARSAT-1 interferometric passes were collected over both sites. The main portions of the interferometric processing of the data, potentially fully automated, provide the magnitude image for each acquisition date (all registered to sub-pixel accuracy), coherence, and (the earth-ellipsoid corrected) phase. The image magnitudes as well as the interferometric coherence both provide a means of easily detecting certain changes in the scene. By assigning the prime colours to sets of three of the magnitude images, and thereby creating an RGB image, even very subtle changes in image magnitudes are easily discernable. The RGB image supplements the coherence image, and together these images offer a potentially valuable tool for wide area surveillance and long term site monitoring. They also provide the timeframe in which the change occurred. These tools take full advantage of RADARSAT-1's wide swath (approximately 50 km in the fine-resolution mode) and systematically repeated orbits.

The RGB magnitude and coherence images were also found to provide contextual information in and around the mine. Signs of change were observed in both mine complexes. However, the rather coarse resolution of RADARSAT-1, and the relatively worse resolution of the coherence image (being a statistical measure of the phase noise) did not permit definitive assessment of these changes.

The later stages of the interferometric processing provides an estimate of terrain subsidence and terrain height, a much more complex process especially for RADARSAT-1 data. The satellite position history need to be known to centimetre-level accuracy. Atmospheric effects can also corrupt the phase data. Due to these factors, and the low resolution of RADARSAT-1, we were not able to obtain accurate elevation, elevation change, or terrain subsidence measurements of the mine complex. But we could conclude that large (coherent) terrain subsidence, which would have left clearly discernable rings patterns in the phase image, was not present.

Mattar, K., 2004, Change detection using RADARSAT-1 interferometry: mine site monitoring, DRDC Ottawa TM 2004-261 Defence R&D Canada – Ottawa

Sommaire

Le présent rapport conclut une étude sur l'application possible de l'interférométrie par satellite à passage répété (SRI) à la détection de changements. L'objectif de ce projet est de développer des outils permettant la surveillance de mines et de surfaces étendues.

Le projet a été en partie soutenu par la Commission canadienne de sûreté nucléaire (CCSN), et a été exécuté en collaboration avec cette dernière. La Commission s'est intéressée à l'imagerie et aux outils qui permettraient la surveillance à distance de mines d'uranium aux fins d'évaluation de la conformité aux traités internationaux. Deux mines d'uranium actives ont été choisies comme sites pour la présente étude : la Range Mine en Australie-Méridionale et la mine Key Lace en Saskatchewan, au Canada. Ces sites furent sélectionnés, à la suggestion de la CCSN, en raison de la possibilité d'obtenir une preuve corroborante. Les sites avaient également fait partie d'études antérieures soutenues par la CCSN.

Plusieurs ensembles de passages interférométriques RADARSAT-1 ont été recueillis sur les deux sites. Les parties principales du traitement interférométrique des données, éventuellement entièrement automatisé, fournissent l'image de la magnitude pour chaque date d'acquisition (chacune enregistrée avec une précision d'une valeur inférieure au pixel), la cohérence et la phase (à correction sphéroïdale). Les magnitudes d'images ainsi que la cohérence interférométrique fournissent un moyen de détecter facilement certains changement de la scène. En assignant les couleurs primaires à des ensembles de trois images de la magnitude, et en créant par conséquent une image RVB, il est facile de discerner de faibles changements dans les magnitudes d'images. L'image RVB complète l'image de cohérence, et ensemble ces images indiquent la période où les changements se sont produits et elles offrent un outil éventuellement précieux pour la surveillance de surfaces étendues et l'observation de sites à long terme. Ces outils profitent de la fauchée large de RADARSAT-1 (environ 50 km dans le mode résolution fine) et des orbites systématiquement répétées.

Les images de cohérence et de magnitude RVB fournissent également des renseignements contextuels de la mine et de ses abords. Des signes de changement ont été observés dans les deux complexes miniers; toutefois, l'imprécision de résolution de RADARSAT-1 et la résolution encore moins précise de l'image de cohérence (étant une mesure statistique du bruit de phase) ont empêché une évaluation finale de ces changements.

Les étapes ultérieures du traitement interférométrique indiquent une approximation de la subsidence et de la hauteur du terrain, un processus très complexe, en particulier dans le cas des données RADARSAT-1, l'historique de la position du satellite devant être connu au centimètre près. Les effets atmosphériques peuvent également corrompre les données de la phase. En raison de ces facteurs et de l'imprécision de la résolution de RADARSAT-1, nous n'avons pu obtenir de mesures précises ni de l'élévation, ni du changement d'élévation ni de la subsidence du terrain du complexe minier. Cependant, nous avons pu conclure à l'absence d'une subsidence du terrain considérable (cohérente), qui aurait laissé des motifs d'anneaux clairement visibles dans l'image de phase.

Mattar, K., 2004, Change detection using RADARSAT-1 interferometry: mine site monitoring, RDDC Ottawa TM 2004-261 R & D pour la défense Canada – Ottawa

Table of contents

This page intentionally left blank.

List of figures

List of tables

This page intentionally left blank.

Acknowledgements

We would like to acknowledge the support of B. Truong and the Canadian Nuclear Safety Commission (CNSC) for this study. The RADARSAT-1 SAR data are copyright CSA (Canadian Space Agency), 2004.

This page intentionally left blank.

Introduction

This study investigates the potential of RADARSAT-1 interferometry for change detection. The study has two central objectives. The first is to evaluate the use of repeat-pass satellite interferometry (SRI) for wide area surveillance and long term site monitoring. The second is to develop tools and assess imagery using SRI for monitoring mine activity. This project was partially supported by, and was carried out in collaboration with, the Canadian Nuclear Safety Commission (CNSC). They are interested in imagery and tools that would permit remote monitoring of uranium mines for the purpose of assessing compliance with international treaties.

The sites considered in this study are Range Mine in South Australia and Key Lakes Mines in Saskatchewan, Canada. These sites were chosen, at the suggestion of CNSC, since they are active mines and because corroborative evidence could potentially be obtained. They were also sites of previous studies supported by CNSC.

Repeat-pass satellite interferometry has been used for accurate digital elevation modelling, for centimetre-level terrain subsidence mapping, for mapping landslides and for estimation of glacier motion, among others [1]. The interferometric coherence in particular has been used, e.g., for mapping floods and monitoring urban areas [1, 2]. Interferometry is, therefore, potentially well suited for monitoring change. Furthermore, the wide swath offered by RADARSAT-1 (approximately 50 km in the fine resolution mode) and multi-frame recording capability of the data means that imagery can cover very large expanses of terrain in a single data collection.

Repeat-pass interferometric SAR overview

The interferometric phase

SAR interferometry requires the collection of two images from nearly the same perspective in space. An interferogram is then calculated using:

$$|z_{\text{int}}|\, e^{j\varphi_{\text{int}}} = |z_{master}|\, e^{j\varphi_{master}} \times |z_{slave}|\, e^{-j\varphi_{slave}} \qquad (1)$$

where $|z_{master}|$, $|z_{slave}|$, and $|z_{mint}|$, are the magnitude of the single look complex (SLC) image of the master, slave, and the interferogram respectively. Similarly φ_{master}, φ_{slave}, and φ_{int} are the phase of the master, slave and interferogram images, respectively. The interferogram phase is essentially a measure of the difference in range between each of the platforms and the ground. Through the use of interferometry, this range difference can be calculated to sub-wavelength accuracy. In the case of RADASAT-1, the wavelength is 5.6 cm.

The interferogram phase contains several potentially desirable as well as undesirable and disruptive components. It can be used to derive the terrain elevation (or target) displacement. The disruptive components include potential ionospheric effects, tropospheric effects, system phase biases, and noise. Mathematically, the interferogram phase is given by [3]:

$$\varphi_{\text{int}} = \varphi_{disp} + \varphi_{topo} + \varphi_{tropo} + \varphi_{ion} + \varphi_{noise} + \varphi_{bias} + 2n\pi \tag{2}$$

where φ_{disp} is the component of the phase due to coherent, line-of-sight displacement of the resolution cell on the ground. Any coherent terrain subsidence will be contained in this phase term. It can be expressed as:

$$\varphi_{disp} = \frac{4\pi}{\lambda}\delta R \tag{3}$$

where δR is the line-of-sight displacement and λ is the wavelength of the radar; φ_{topo} is the component of the phase due to topography and can be given by:

$$\varphi_{topo} = \frac{4\pi B_{\perp}}{\lambda R \sin(\theta)} h + \varphi_{ellipse} \tag{4}$$

where h is the elevation above the ellipsoid, $B_{\perp}$ is the perpendicular component of the baseline, R is the slant range between the designated master platform and the target on the ground, and θ is the incidence angle; φ_{tropo} represents the component of the phase due to extraneous tropospheric effects; φ_{ion} represents the component of the phase due to ionospheric electron density fluctuations; φ_{noise} represents other noise sources such as system noise and scene decorrelation; $\varphi_{ellipse}$ is the relevant ellipsoidal model of the earth; and φ_{bias} accounts for the phase bias between the master and slave.

The coherence

Coherence is a measure of the degree of correlation between two single look complex images. It is a measure of the phase noise within a given window of pixels. It can also be described as a measure of the macroscopic changes in a scene. A couple of examples may be helpful. Consider InSAR measurement of a landslide [5] or mine subsidence [6]. If the ground that makes up the landslide or mine undergoes subsidence without changing the radar signature of the scatterers (i.e., just displacing them) then the coherence will remain high and the displacement will contribute to the displacement phase modelled by (3). If the radar signature is changed, for example by disturbance or crumbling of the rocks that make up the landslide or mine surface, then the phase may be randomized and the coherence lost. The degree of loss of coherence will depend on the extent to which the ground scatterers are disturbed relative to the perspective of the radar.

As a statistical measurement, the coherence is calculated over a window of samples. Hence it always has lower spatial resolution as compared with the magnitude or phase images. The coherence varies between "0" and "1": "0" (usually imaged as black) signifies complete decorrelation between the two scenes; "1" (usually imaged as white) signifies perfect correlation. Mathematically the interferometric coherence magnitude, δ, can be estimated by a sample statistic given by [7]:

$$\delta = \frac{\left| \sum_{i=1}^{L} z_{1i} z_{2i}^{*} \right|}{\sqrt{\sum_{i=1}^{L} \left| z_{1i} \right|^{2}} \sqrt{\sum_{i=1}^{L} \left| z_{2i} \right|^{2}}} \tag{5}$$

where i is the sample number, L is the number of samples in the coherence window, and z_1 and z_2 are the two single look complex images.

The number of samples used in the coherence window is an important consideration [5]. The ***apparent*** coherence will vary depending on the size of the window (L) over which the statistical averaging is carried out. The variation in the apparent coherence is most significant for small windows, and begins to level off above an L of 40 to 50 [7].

To find the ***true*** or ***absolute*** coherence for an area, a sufficiently large coherence window must be used or the coherence must be calibrated as described in [7]. The ***absolute*** coherence has been used in the classification of a variety of targets and features [7,8].

Causes of scene decorrelation

Coherence has become an important tool within repeat-pass Satellite Radar Interferometry. It is also a key limitation in the dependability of SRI applications. There are many factors that can cause degradation in the scene coherence. Consequently, at best, these limit the resolution and usefulness of SRI applications and, at worst, completely prevent them. It is useful to list some of these decorrelation factors and examine means of overcoming, or at least reducing them where possible. The total observed correlation δ_{total}, or decorrelation $(1-\delta_{total})$ can be given in terms of the product of some of the more significant correlation factors [9]:

$$\delta_{total} = \delta_{thermal} \times \delta_{temporal} \times \delta_{baseline} \times \delta_{troposphere} \times \delta_{ionosphere} \times \delta_{coregistration} \times \delta_{volume}. \tag{6}$$

We now consider each of these correlation factors separately.

Thermal: $\delta_{thermal}$ is the thermal correlation coefficient and is a function of the thermal noise of the two systems. It is given by [9]:

$$\delta_{thermal} = 1/(1+SNR^{-1}), \tag{7}$$

where SNR is the signal-to-noise ratio of the system. Obviously, for any given system, this value normally does not vary.

Temporal: $\delta_{temporal}$ is the temporal correlation coefficient. It is one of the more detrimental factors in SRI. It would include, for example, any changes in moisture of the terrain due to precipitation, and random movement of the prime reflective components of vegetation or forest cover. Many (but not all) of these factors are highly dependent on the wavelength of the system. For example, at X-band, the main scatter from a tree may be due to the small

branches and leaves. At larger wavelengths, such as L-band, the main scatter of the tree may be from the trunk, which is less susceptible to movement. Therefore, depending on the circumstances, the temporal decorrelation coefficient may be reduced by using a longer wavelength radar (e.g. L- or P-band), by reducing the time interval between acquisitions of the interferometric pair, or by repeated trials hoping that one pair will have a sufficiently low decorrelation.

Baseline: $\delta_{baseline}$ is the baseline correlation coefficient. It is maximum when the two antennae that make up the InSAR pair view the ground scatterer from the same viewing angles (though not necessary from the same distance). This occurs when the component of the baseline perpendicular to the range direction of the master satellite ($B_{\perp}$) is zero. As the perpendicular baseline increases, the ground reflectivity spectra acquired by the two antennae becomes increasingly divergent, the scene coherence is reduced, and the baseline correlation coefficient decreases. Beyond a certain critical value (called the critical baseline), the Doppler spectra of the interferometric pair no longer overlap, and the coherence between the pair is completely lost. The critical baseline, $B_{\perp, cr}$, is given by [10]:

$$B_{\perp, cr} = \lambda R \tan\theta / 2R_r , \tag{8}$$

where R_r is the slant range resolution, λ is the wavelength, R is the slant range, and θ is the nominal incidence angle. For ERS-1/2, for example, this critical baseline is approximately 1100 meters.

When the perpendicular baseline lies between these two extremes, bandpass filtering can be used to select the common portions of the reflectivity spectra. This will increase the scene coherence, but at the expense of resolution.

Troposphere: Tropospheric decorrelation, $(1-\delta_{troposphere})$ is among the more difficult decorrelation factors to reduce, let alone predict. In some cases it is observed as a ghost-like figure in the coherence map. In other cases, as with atmospheric gravity waves, a distinctive pattern can be observed in the interferogram phase, and once detected can be reduced by an appropriately designed filter. In most cases, the tropospheric effects on any given interferogram are subtler but by no means less significant [11]. If a reference digital elevation model (DEM) is available, the difference in slant range between the measured interferogram phase and the topographic phase (as calculated from the DEM) may reveal the existence and magnitude of any tropospheric effects. The user may then be able to judge the significance of the effect and, if serious, can either find a better pair or attempt to improve the existing one by filtering. In practice, tropospheric problems often remain unnoticed, with consequent degradation to the accuracy of the final results.

Ionosphere: Ionospheric decorrelation $(1-\delta_{ionosphere})$ is less serious than the tropospheric decorrelation. Its distinctive linear "streaking" pattern is often clearly visible in the coherence map. The magnitude of the effect can be estimated by calculating a map of the azimuth shift needed for optimal coherence. In DEM generation applications, the azimuth shift can also be used in a first order correction of the interferogram phase.

Co-registration: $\delta_{coregistration}$ refers to the coherence factor due to linear and circular co-registration errors between the master and slave images. This can be an important factor in SARs operating with a squint. For example, for a RADARSAT-1 system operating in stripmap mode with a yaw angle of 3 degrees, an interferometric phase error of about 30 degrees occurs from near to far range if the interferometric pair is misregistered by 0.1 sample in azimuth [12].

Volume: Finally, $(1-\delta_{volume})$ is the volume decorrelation factor. This would include decorrelation due to multi-path scattering, scattering from two or more differing surfaces within a volume, such as the leaves and trunk of trees in a forest, or from the air/ice interface and interface between differing ice layers within a glacier in the Antarctic.

This is, by no means, an exhaustive list of decorrelation factors. Not included in the above list, for example, is decorrelation due to systematic processing errors.

Non coherent change

As indicated in the previous section, there are a variety of factors that can adversely influence the scene coherence. A loss of scene coherence does signify a change of some sort. But identifying exactly the source of that change can be difficult. An additional source of change information is the difference in magnitude of the two images used to form the interferogram. It can be used to supplement the coherent change information, and will provide change information even in the complete absence of scene coherence. The two magnitude images are registered to sub-pixel accuracy by virtue of the InSAR processing. With very little additional processing the two (or in the case of an interferometric triplet, three) different magnitude images can be represented in colour as an RGB image. Even subtle magnitude changes are readily visible in this RGB magnitude change image. Furthermore, by virtue of the small separation between the baseline, the stereo effect is insignificant. This helps avoid misinterpretation of a change in local topography as a change in the ground scatterer.

Detecting ground deformation and terrain height changes

The terrain elevation can be readily derived using (4) and (2):

$$h = \frac{\lambda R \sin(\theta)}{4\pi B_{\perp}} \left(\varphi_{\text{int}} - \varphi_{ellipse} - \varphi_{disp} - \varphi_{tropo} - \varphi_{ion} - \varphi_{noise} - \varphi_{bias} - 2n\pi \right) \tag{9}$$

But solving for h requires knowledge of the terrain subsidence. The terrain height and terrain subsidence both contribute to the interferogram phase. They can be separated with an interferometric triplet and a few assumptions. Given one master and two slaves, let us assume that the two slaves surround the master in time. Furthermore, let us assume that the ground deformation is constant during the entire interval in question, that the ground height has not changed, and, for simplicity, that the atmospheric effects can be ignored. Then, for each pair in the triplet, (9) can be written as:

$$h = \frac{\lambda R \sin(\theta)}{4\pi B_{\perp 1}} \left(\varphi_{\text{int}1} - \varphi_{ellipse} - \varphi_{disp} - \varphi_{bias1} - 2n_1\pi \right) \tag{10}$$

and,

$$h = \frac{\lambda R \sin(\theta)}{4\pi B_{\perp 2}} \left(\varphi_{\text{int}2} - \varphi_{ellipse} + \varphi_{disp} - \varphi_{bias2} - 2n_2\pi \right) \tag{11}$$

Subtracting (10) and (11) and solving for the displacement gives:

$$\varphi_{disp} = \frac{B_{\perp 1}\left(\varphi_{\text{int}2} - \varphi_{ellipse} - \varphi_{bias2} - 2n_2\pi \right) - B_{\perp 2}\left(\varphi_{\text{int}} - \varphi_{ellipse} - \varphi_{bias1} - 2n_1\pi \right)}{B_{\perp 1} + B_{\perp 2}} \tag{12}$$

The height can then be calculated using either (10) or (11).

On the other hand, we could assume that the displacement is negligible but that the ground height may have changed between the successive passes. In this case, height h in (10) and (11) may be different; subtracting them gives an estimate of the change in height, Δh:

$$\Delta h = \frac{\lambda R \sin(\theta)}{4\pi} \left(\frac{\varphi_{\text{int}1} - \varphi_{ellipse} - \varphi_{bias1} - 2n_1\pi}{B_{\perp 1}} - \frac{\varphi_{\text{int}2} - \varphi_{ellipse} - \varphi_{bias2} - 2n_2\pi}{B_{\perp 2}} \right) \tag{13}$$

Accuracy issues

The accuracy of the calculated height derivation will depend on the accuracy of our knowledge of the various parameters and phase terms listed in the original equations (2) and (4). Several among these are the more critical. Accurate, centimetre-level knowledge of $B_\perp$ is essential. This in turn requires accurate knowledge of the position history of the two platforms at the time of image acquisition. The orbits of ERS and ENVISAT are known to the decimetre level [13,14]. But even this is not accurate enough for SRI. By contrast the orbit of RADARSAT-1 is known only to within 50 m [15]. In either case a calibration procedure, requiring some terrain height information, is required to improve estimation of the baseline.

Tropospheric phase effects often contribute significantly to the interferogram phase [16]. They are unpredictable and cannot be directly measured to the required resolution. By contrast the presence, and strength, of ionospheric phase effects in the interferogram can be assessed [10]. If they are present, filtering can sometimes be used to remove first order effects [10]. The user could also choose to acquire another, more suitable InSAR pair.

Finally, phase biases can be determined through the use of a Ground Control Point (GCP) within the scene [1].

Similarly, accuracy of the ground deformation estimation will depend on the various parameters in (2). Principal among these are the tropospheric effects, ionospheric effects, and

phase noise. If only one InSAR pair is available, then a terrain elevation model will be required. Errors in the elevation model may be misinterpreted as terrain subsidence.

Large terrain (coherent) subsidence (large relative to the 5.6 cm wavelength of the radar), appear as very distinctive ring-like patterns in the phase image [1]. These are sometimes clearly discernable despite the presence of significant atmospheric effects and possible errors in the model of the terrain topography [1].

Repeat-pass interferometric SAR processing

The flow chart for InSAR processing is shown is shown in Figure 1. All the tasks, with the exception of the starred (*) items can readily be automated. The tasks with a star (*) are more difficult and often require manual intervention. A detailed description of the processing steps is outside of the scope of this report. Input to the chain are the focused image pair with their relevant parameters and orbit history information. The first outputs of the process include the two magnitude images from which a two colour magnitude change image can be readily obtained. The other outputs include the coherence and the ellipsoid-corrected interferogram phase. Processing to this point can be fully automated in a fairly robust fashion. The two-colour (or three-coloured) magnitude change image and the coherence can potentially be a useful tool for wide-area change monitoring.

The subsequent stages and the potentially manually intensive portion of the processing are required for accurate estimation of the terrain height and/or terrain subsidence. These artefacts were described in detail in the previous section. The greater the desired accuracy, the more stringent are the requirements on calibration and atmospheric correction. Conversely, in cases where (coherent) terrain subsidence is large (large in comparison with the wavelength of the radar) very distinctive deformation rings may be evident in the interferogram phase.

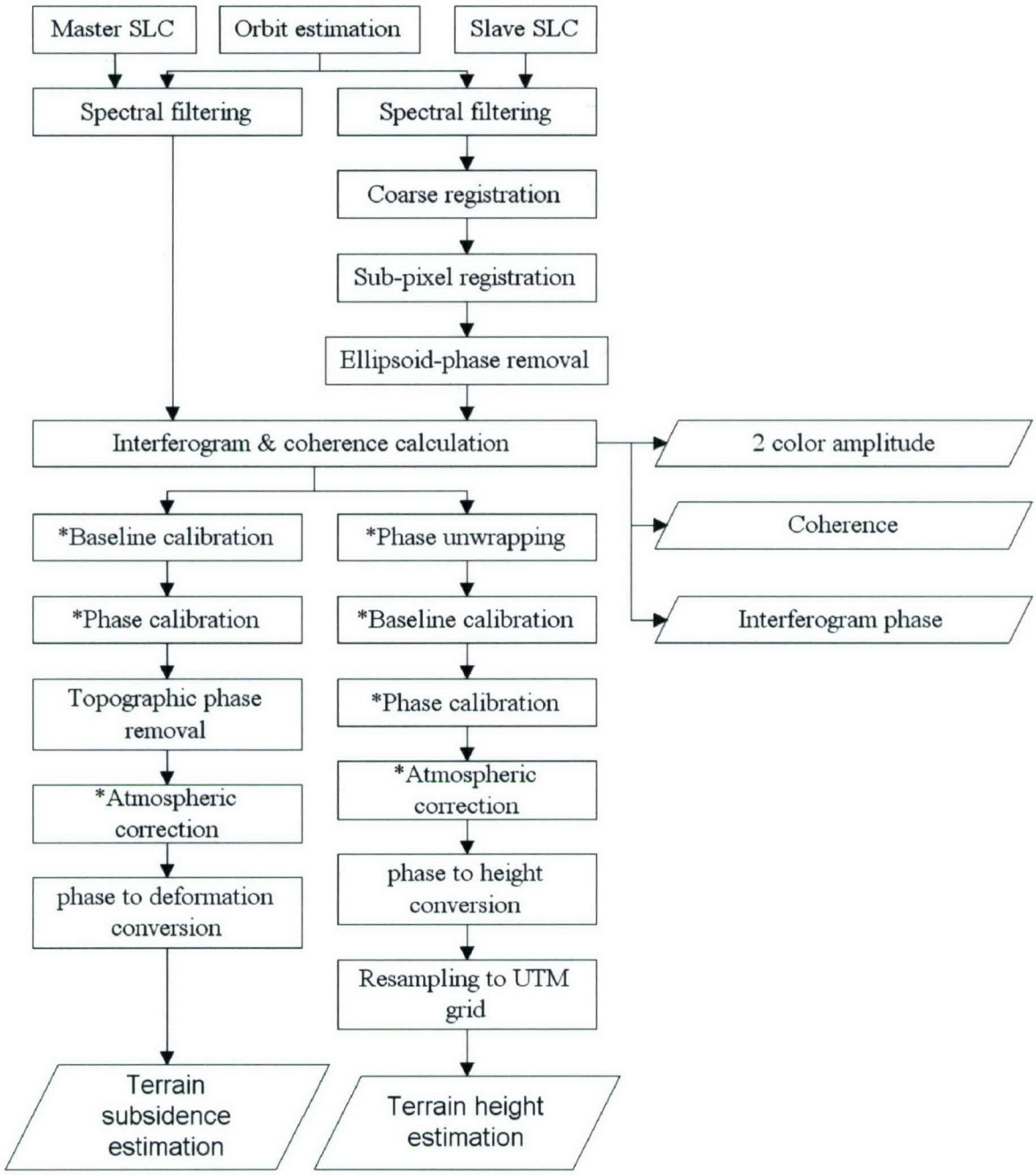

Figure 1: Flowchart of the InSAR processing. All the tasks, with the exception of the starred (*) items can be readily automated. The stared items are more difficult tasks often requiring manual intervention.

Range Mine, Australia

Range Mine is an active uranium mine located in South Australia. In total, seven RADARSAT-1 images were acquired, four ascending passes (south to north) and three descending passes (north to south). The pertinent information about these passes is listed in Table 1. The four ascending passes form an interferometric quadruplet, while the three descending passes form an interferometric triplet. Information about the absolute distance between any of the platforms that form the two interferometric pair (referred to as the 3D baseline, or B_{3D}) is listed in Table 2. The critical baseline ($\mathbf{B}_{CR}$) was calculated using (8). Of all the passes, the March 8 – April 25 pair has the largest perpendicular baseline, $\mathbf{B}_{\perp}$. Although it is small compared with the critical baseline, it large enough to cause substantial baseline decorrelation, and consequently is not suitable for interferometry. $\mathbf{B}_{VEL}$ is the component of the baseline parallel to the velocity vector of the master. A non-zero value, as is the case for all these passes, is an indication that the platform trajectories are not parallel. $\Delta\mathbf{H}_{2\pi}$ is a measure of the terrain elevation to phase sensitivity. It is the terrain elevation calculation based on an interferometric phase of 2π. It was calculated using (4) by substituting 2π for the phase φ_{topo}. The nominal information on the F4F mode of RADARSAT-1, used for all the acquisitions in this report, is given in Table 3.

Table 1: RADARSAT-1 data acquired over Range Mine

INTERFEROMETRIC DATA (2003)	DAY OF THE YEAR 2003	START TIME (GMT)	BEAM POSITION	INCIDENCE ANGLE AT SCENE CENTRE (DEGREES)	PASS	ORBIT #
Feb 12	42	09:40:19.406	F4F	44.8	Asc	37970
Mar 8	67	09:40:19.452	F4F	44.8	Asc	38313
Apr 1	91	09:40:14.287	F4F	44.8	Asc	38656
Apr 25	115	09:40:11.188	F4F	44.8	Asc	38999
Feb 2	33	20:34:30.285	F4F	45.1	Desc	37834
Feb 26	57	20:34:27.018	F4F	45.1	Desc	37177
Mar 22	81	20:34:27.213	F4F	45.1	Desc	38520

Table 2: Interferometric details of Range Mine dataset relative to scene centre

INTERFEROMETRIC PAIR (2003)	B_{3D} (M)	B_{VEL} (M)	$B_{\perp}$ (M)	$B_{\parallel}$ (M)	B_{CR} (M)	$\Delta H_{2\pi}$(M)
Feb 12 – Mar 8	577	+23	−433	−381	6073	49.2
Feb 12 – Apr 1	1051	−39	+855	+609	6073	24.9
Mar 8 – Apr 1	1625	−61	+1288	+989	6074	16.6
Mar 8 – Apr 25	2496	−85	1938	+1570	6071	11.0
Apr 1 – Apr 25	873	−24	+650	+583	6073	32.8
Feb 2 – Feb 26	725	−36	+553	−468	6144	37.8
Feb 2 – Mar 22	136	−29	−120	−57	6144	169.4
Feb 26 – Mar 22	597	+7	+433	+411	6142	48.3

Table 3: Pertinent information about RADARSAT-1's F4F mode

Slant range spacing (m)	4.6
Ground range spacing (m; at scene centre)	6.6
Azimuth spacing (m)	5.0
Slant range resolution (m)	5.6
Ground range resolution (m; at scene centre)	7.9
Azimuth resolution (m; dependent on spectral filtering)	8.9-10.8
Swath width (km)	50
Approximate incidence angle range (degrees)	43.6-46.0

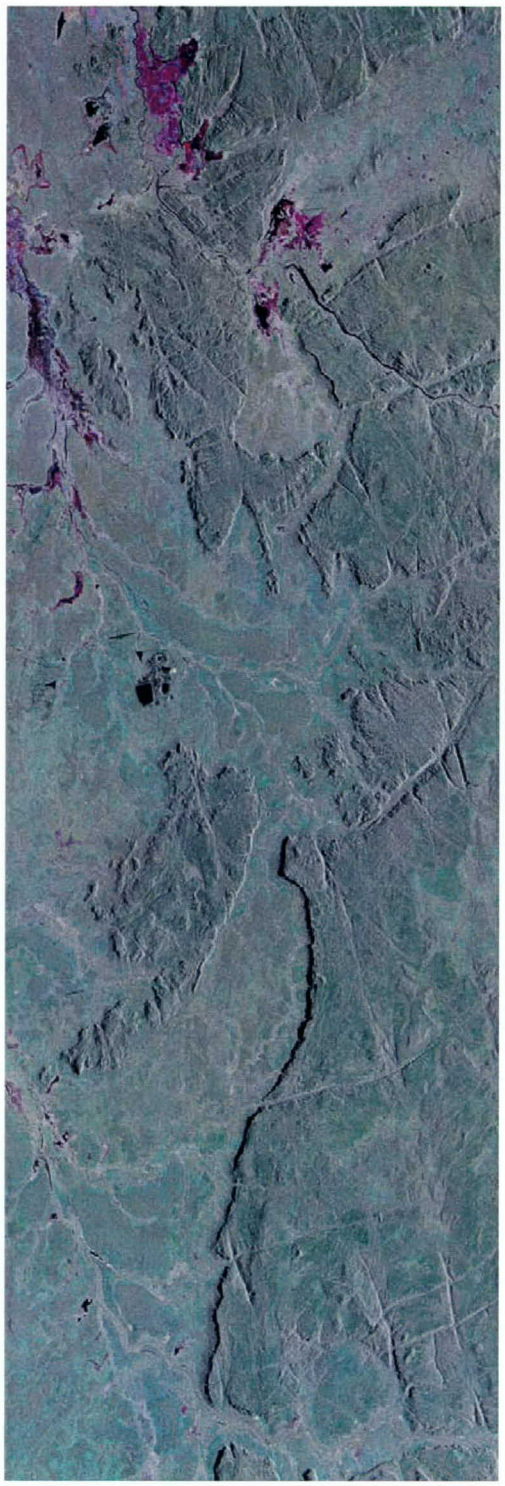

Figure 2: Magnitudes from 2 February (red), 26 February (green), and 22 March (blue) 2003 covering an area 82 km x 36 km.

Figure 3: Magnitudes from 12 February (red), 8 March (green), and 1 April (blue) 2003 covering an area 81 km x 36 km.

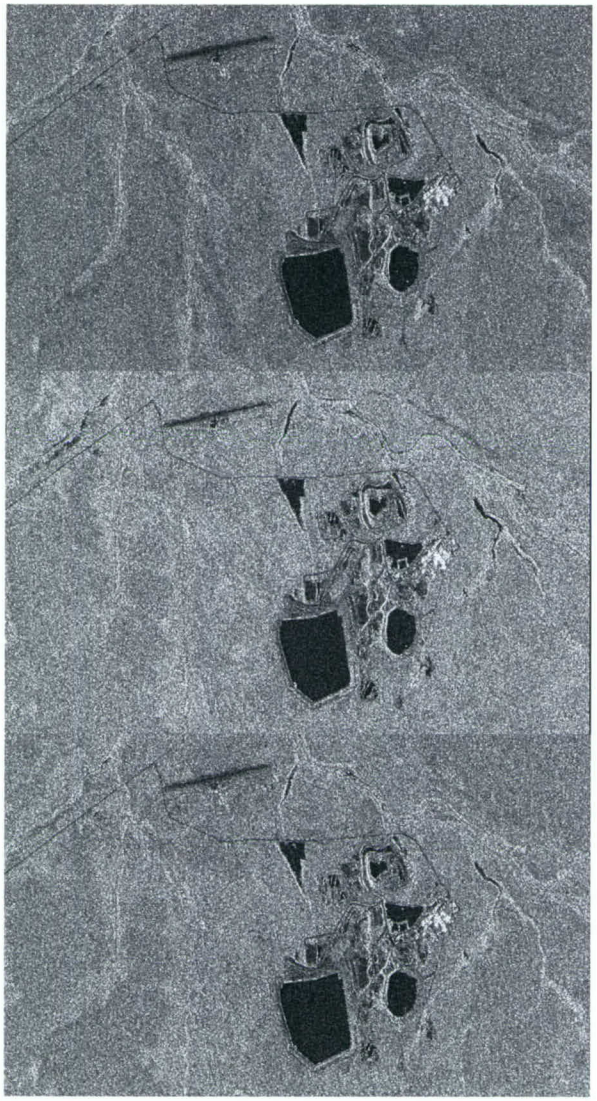

Figure 4: Range Mine magnitude. From top 2 February, 26 February, and 22 March 2003.

InSAR processing of the data sets proceeded as outlined in Figure 1. An RGB image of the magnitudes from the 2 February (red), 26 February (green), and 22 March (blue) passes is shown in Figure 2. The equivalent RGB image of the magnitude from the 12 February (red), 8 March (green), and 1 April (blue) passes is shown in Figure 3. Change in the scene is visible in colour. Lack of any change among the three passes shows up as a shade of grey. The colour of the change itself may provide some indication of **when** the change took place. Consider Figure 2; An object that is **brighter** in the 2 February magnitude image compared with the other two passes will appear red in the RGB image. Conversely an object that is **darker** in the 2 February magnitude image compared with the other two passes will lack red

and, therefore, appear cyan. The colour wheel is given in Figure 6, and may aid with colour interpretation.

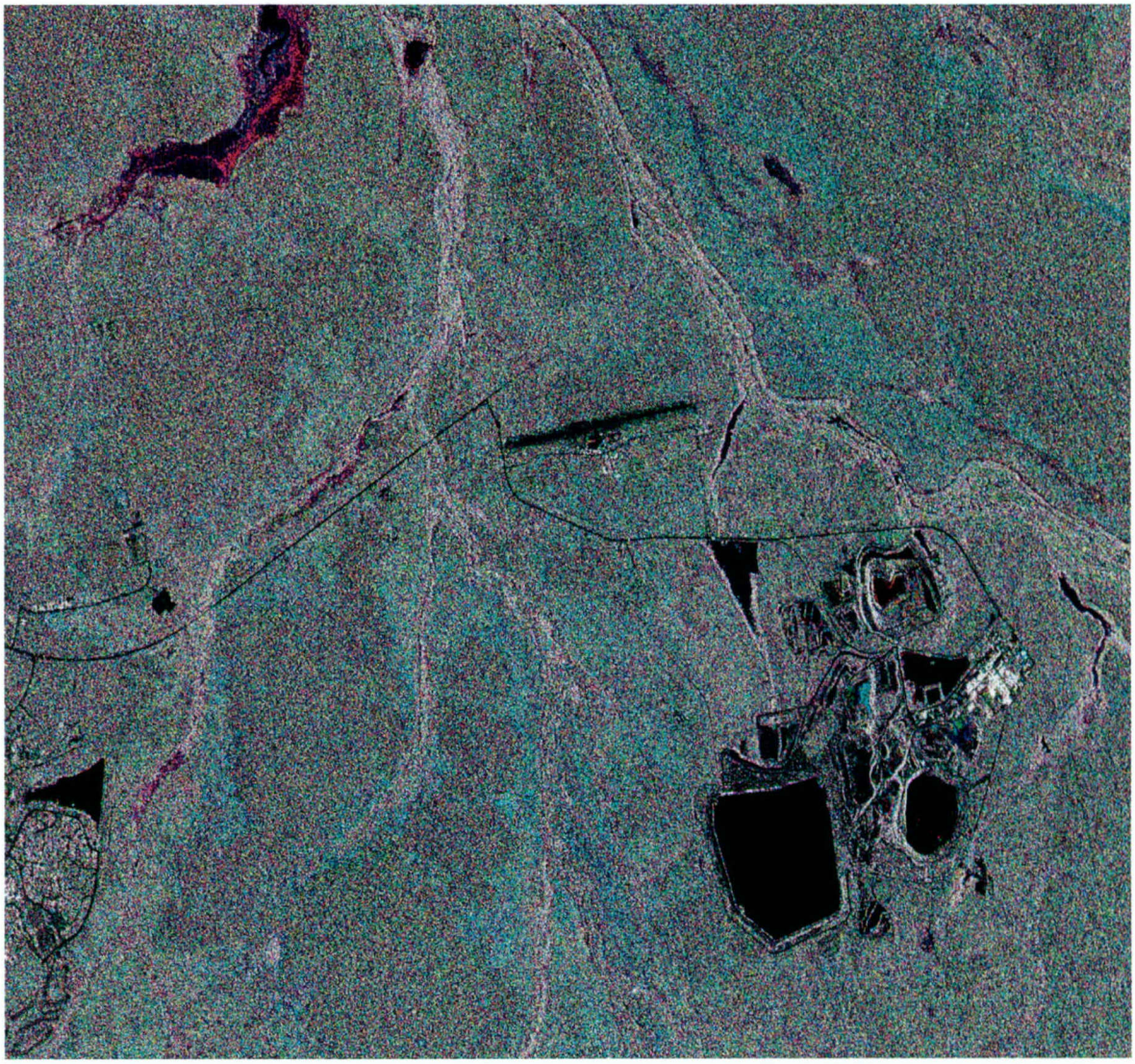

Figure 5: Full resolution Range Mine magnitude images from 2 February (red), 26 February (green), and 22 March (blue) 2003.

The RGB images permit discrimination of large as well as **very subtle** changes between the three images. Some of these changes reflect system problems; others represent real changes on the ground. Figure 2 has an overall tinge of green indicating a subtle difference in the radiometry of one or more of the three passes. The orange tinge and two purple bands visible in Figure 3 indicate a more serious radiometric calibration problem, perhaps due to a gyration of the satellites at the time of image acquisition. These radiometric calibration problems do not hinder the interpretation of other changes visible in the scene. Evidence of flooding is visible, especially in the upper portion of both figures. Flooding in this general area has been corroborated by others [17] and is evident from the precipitation record, shown in Figure 9. This precipitation record was collected by Jabir airport near the mine. The subtle variations in

the tones of green and cyan visible in Figure 2 are possibly indicative of ground saturation. Many other small changes are visible, but require a full resolution version of the above two figures. One of the more interesting changes in what appears to be a farmed region, visible in the upper left portion of Figure 2, is shown in full resolution in Figure 8.

Range Mine is visible in the left of the central portion of Figure 2 & Figure 3. It is shown in full resolution in Figure 5 & Figure 7. To aid in the interpretation of the RGB image, the three separate magnitude images from 2 February (top), 26 February (middle), and 22 March (bottom) are shown in Figure 4.

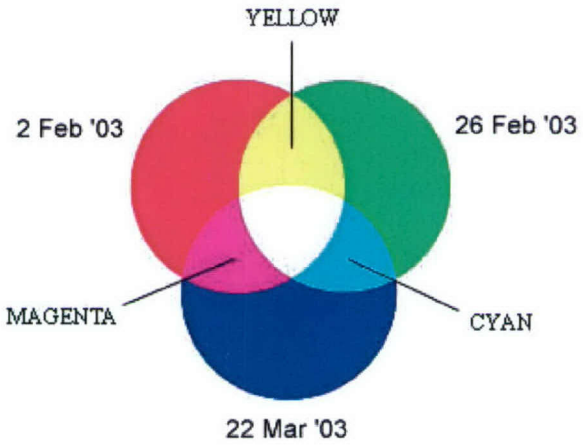

Figure 6: RGB colour wheel used in Figure 2, Figure 5 & Figure 8. For Figure 3 & Figure 7 replace 2 Feb, 26 February and 22 March with 12 Feb, 8 March, and 1 April.

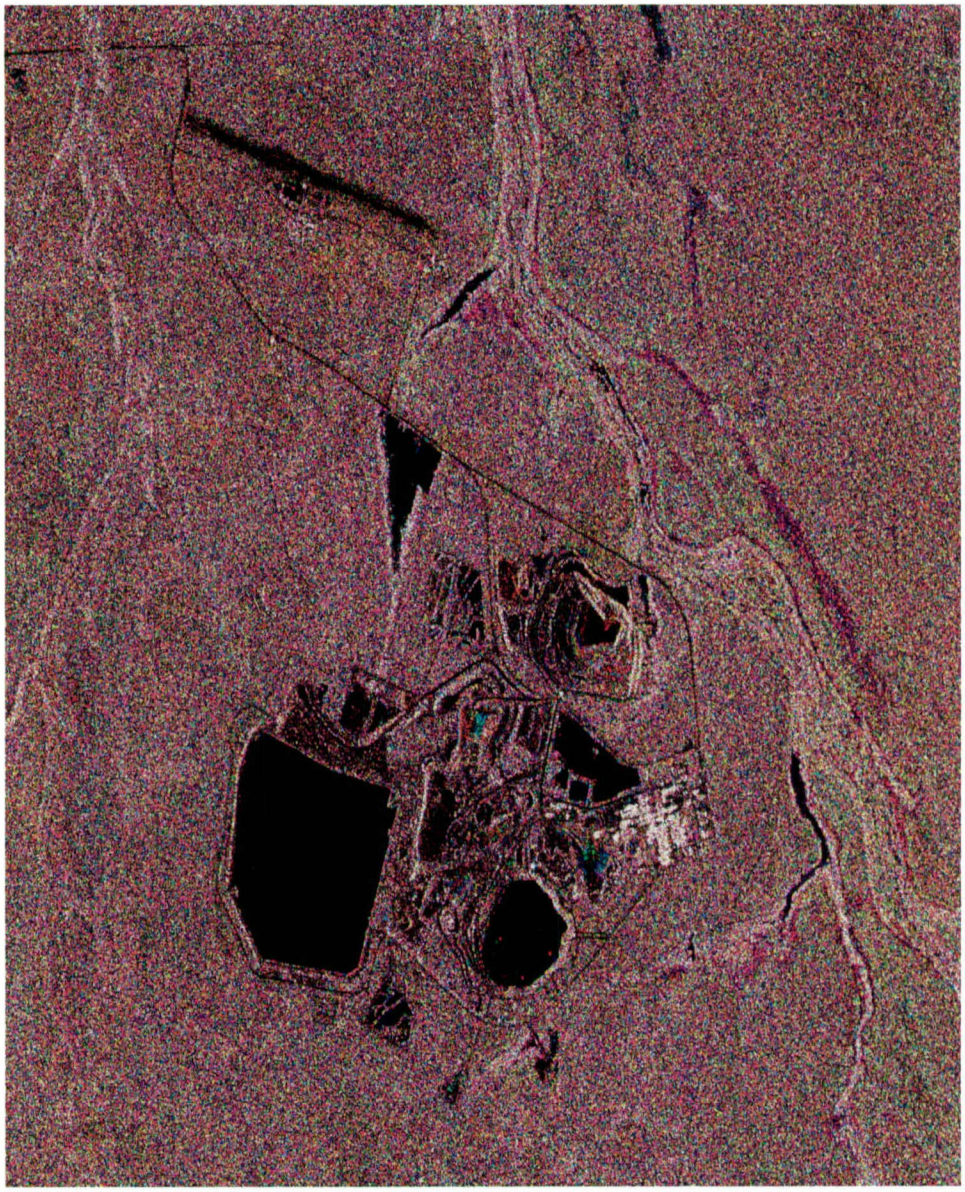

Figure 7: Full resolution Range Mine magnitude images from 12 February (red), 8 March (green), and 1 April (blue) 2003.

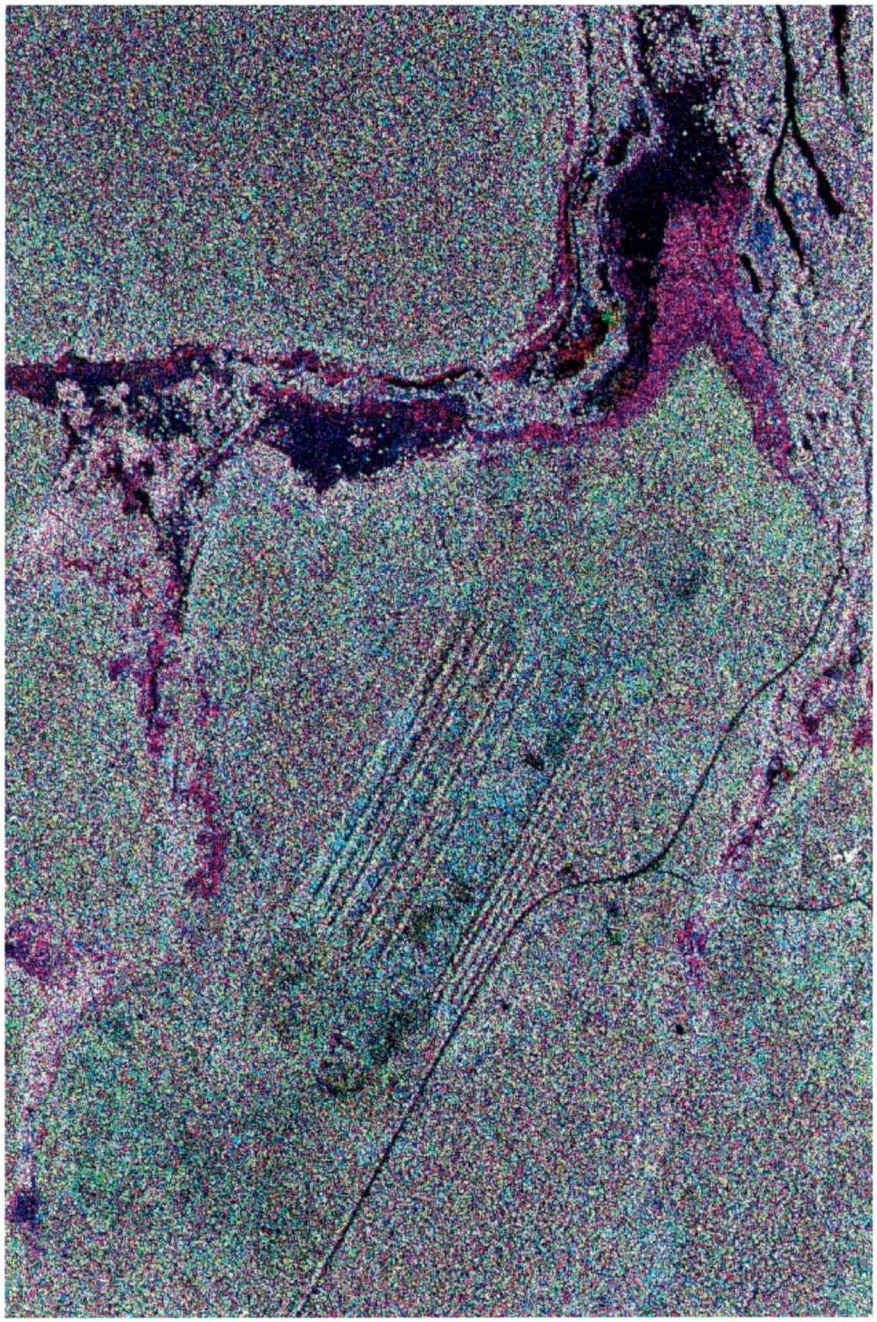

Figure 8: Detail from Figure 2 in full resolution with magnitudes from 2 February (red), 26 February (green), and 22 March (blue) 2003, covering an area approximately 4.1 km x 5.8 km..

Examining Figure 5 in more detail, a large area of flooding is visible northwest of the airport and smaller areas of flooding are visible in other portions of the image, some relatively close to the mine complex and airport. The flooding appears mainly as magenta, or a lack of green (since flooding shows up as a relatively dark area in the magnitude image). This signifies that it is largely visible in the 26 February image. Portions of the flooding appear red and are in

fact visible in both the 26 February and 22 March images. The subtle colour variations in green-teal tinge visible in large portions of the image may signify ground saturation. The same interpretation can be made from Figure 7.

Range mine shows some signs of change in both RGB images. Two small areas of change are clearly visible. The first is located just above the central portion of the mine site. In Figure 5 the area is cyan with some green. The second is located right of centre. It is purple coloured and appears to contain some green. The same two areas are distinguishable in Figure 7.

The precise nature of this change is difficult to interpret. It may be a change due to object or material that has been removed or added to the ground. In the context of the flooding, which surrounds the mine, the apparent change may also be caused by increased moisture content in the soil.

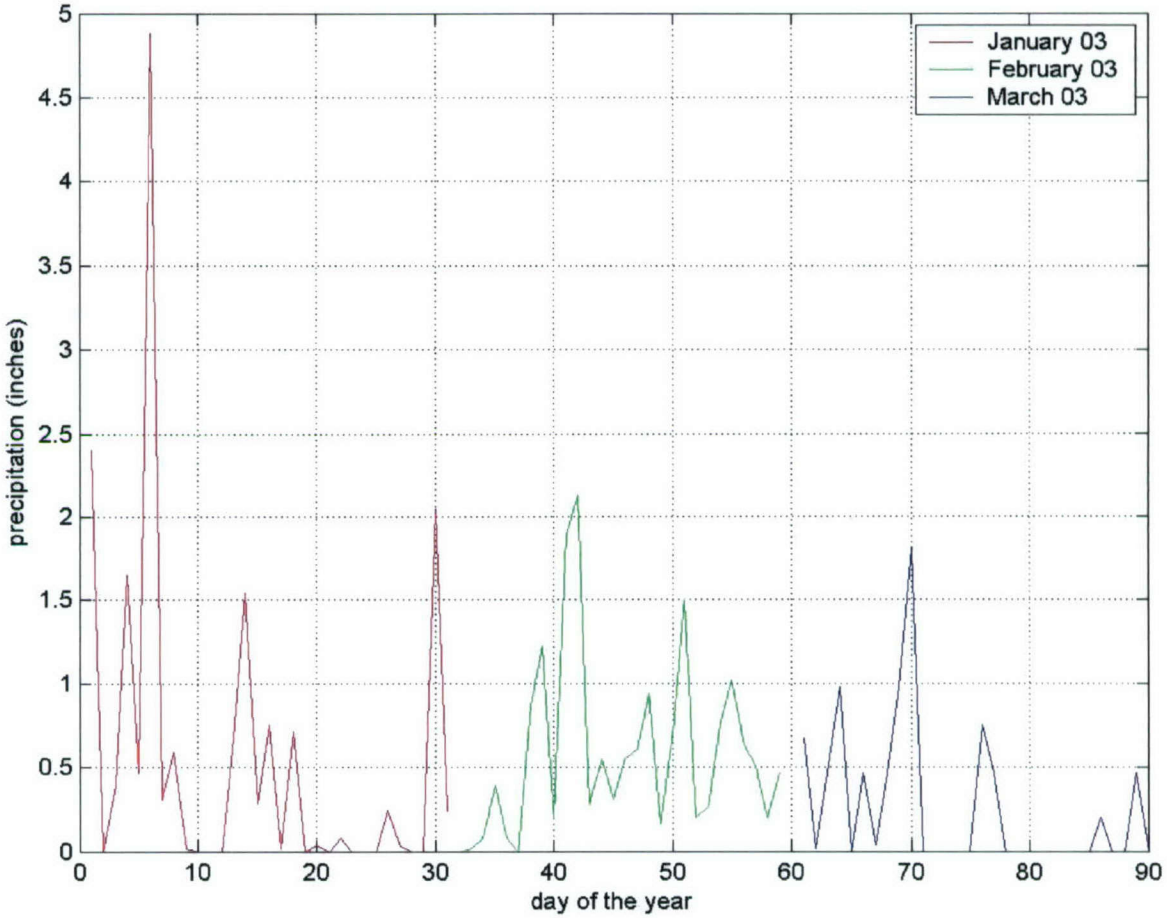

Figure 9: Precipitation at Jabir airport, located 2.6 km from Range Mine, for January, February and March 2003.

The interferometric coherence often can be very helpful with the interpretation. Unfortunately, due no doubt to the flooding and change in moisture content of the soil, the general area covered in these images lacked coherence. Only very isolated areas of the scene

were coherent. An attempt was made to calculate the change in height for those areas of the mine that did provide some phase information (see Figure 10). Following (13), the height difference between the 26February/2February and 26February/22March InSAR pair was calculated following the procedure outlined in Figure 1. The few and isolated areas with phase information prevented adequate phase unwrapping. The lack of ground control points (GCPs) and the unwrapping difficulties due to the phase noise did not permit an accurate baseline or phase calibration. Speckle correlation test [10] demonstrated that ionospheric phase effects were negligible for all these data sets. No assessment was possible concerning the presence of any tropospheric phase effects. The estimated elevation difference shown in Figure 10 is for these reasons suspect. No firm assessment of the change in the mine area, or increase of the pilings near the mine, can be made. The only firm conclusion that can be drawn from this phase data is that large ground deformations are not present. Terrain subsidence even at the decimetre level, would form very characteristic circular banding, or ring-like patterns in the phase image. These are not visible.

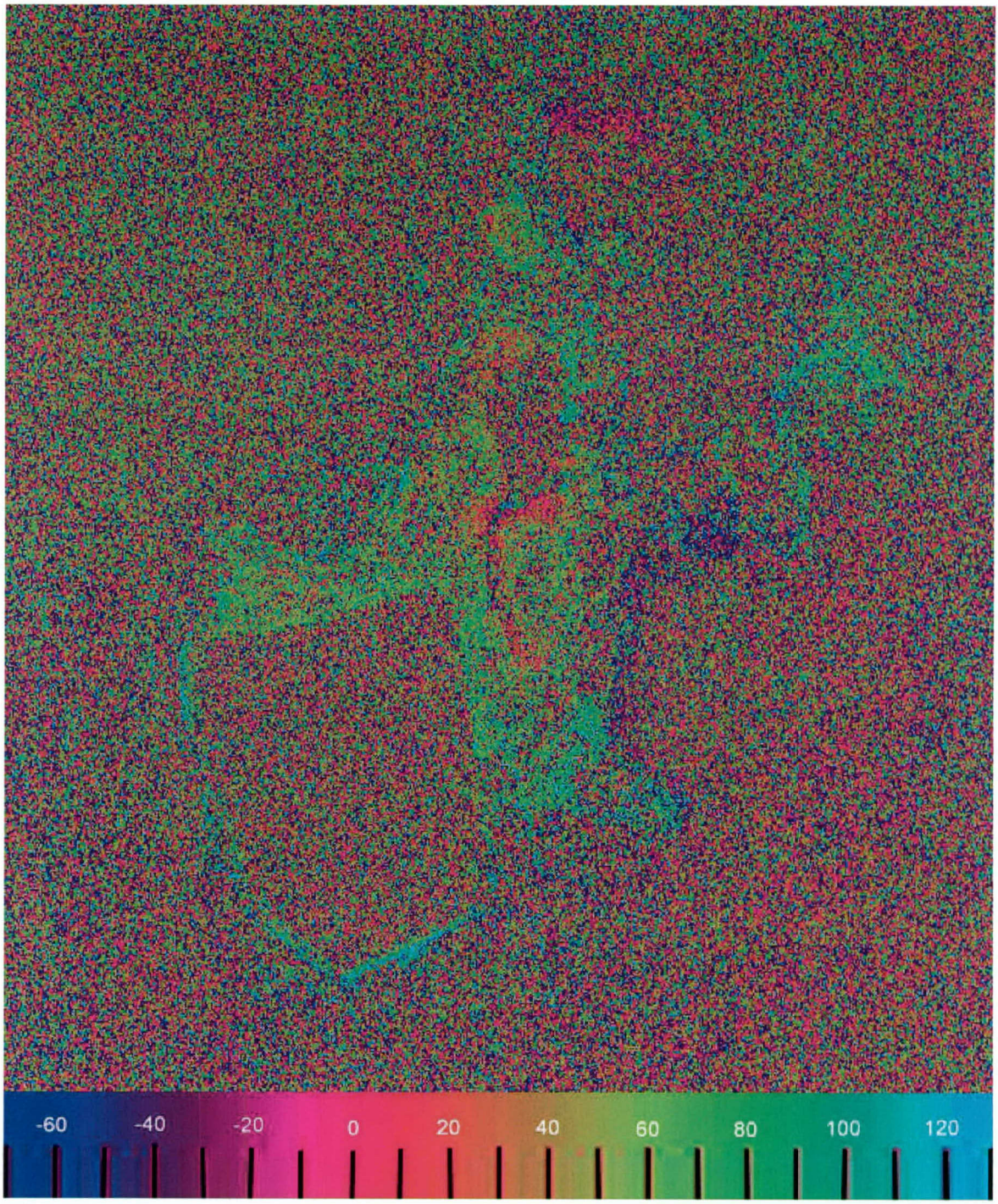

Figure 10: Height difference (in meters) between the 26February/2February and 26February/22March InSAR pairs. The lack of ground control points and unwrapping difficulties did not permit an accurate baseline and phase calibration.

Key Lake, Saskatchewan

Key Lake, Saskatchewan, is the second site of this study. In total, five ascending RADARSAT-1 images were acquired. Some of the pertinent information about these passes is listed in Table 4. The five images were acquired at 24 day intervals from July 28 to November 1, 2003 and form an interferometric quintuplet. The Pulse Repetition Frequency (PRF) is usually exactly the same for interferometric datasets. This case was an exception. The PRF for two of the passes in this set differed from the other three by 0.3288 Hz. New software had to be written to resample the data to account for this difference. The additional processing step was inserted just prior to the "coarse registration" step in Figure 1. The remaining processing steps proceeded normally.

Table 4: RADARSAT-1 data acquired over Key Lake

INTERFEROMETRIC DATA (2003)	DAY OF THE YEAR 2003	START TIME (GMT)	BEAM MODE	INCIDENCE ANGLE ESTIMATE AT SCENE CENTRE (DEGREES)	PASS	ORBIT	ORIGINAL DOPPLER CENTROID OFFSET AT SCENE CENTRE, (HZ)	PRF (HZ)
Jul 28	209	0:54:02.43138	F4F	44.817	Asc	40338	−6102.6	1330.91
Aug 21	233	0:53:59.80838	F4F	44.821	Asc	40681	−6170.0	1330.91
Sep 14	257	0:53:55.58402	F4F	44.831	Asc	41024	−6226.3	1330.58
Oct 8	281	0:53:54.50802	F4F	44.826	Asc	41367	−6272.0	1330.58
Nov 1	305	0:53:53.65913	F4F	44.819	Asc	41710	−6268.2	1330.91

Table 5: Interferometric details of Key Lake dataset relative to scene centre

INTERFEROMETRIC PAIR (2003)	B_{3D} (M)	B_{VEL} (M)	$B_{\perp}$ (M)	$B_{\parallel}$ (M)	B_{CRIT} (M)	$\Delta H_{2\pi}$(M)
Aug 21 – Jul 28	299	−16.5	+214	+208	6094	97.3
Jul 28 – Sep 14	362	+132	+295	+165	6095	70.6
Jul 28 – Oct 8	186	+115	+126	+73	6095	165
Aug 21 – Sep 14	641	+116	+509	+372	6094	40.9
Aug 21 – Oct 8	452	+98	+340	+281	6094	61.2
Sep 14 – Oct 8	192	−17.8	-169	−90	6091	123

Of the five passes, the November 1 dataset did not show any coherence with any of the other four passes. The weather data acquired at the airport closest to the mine (and visible in the imagery) is shown in Figure 11, and provides an explanation for the decorrelation. Precipitation was fairly consistent throughout the period of acquisition. However, while the temperatures remained well above freezing throughout the first 4 acquisitions, they fell to near freezing or below freezing for the duration of the two weeks prior to the last acquisition. It therefore can be presumed that during this period the precipitation fell as snow, and by the November 1 acquisitions the snow had accumulated to a degree that affected the radar return.

The change in radar backscatter was sufficient to cause decorrelation with all prior acquisitions.

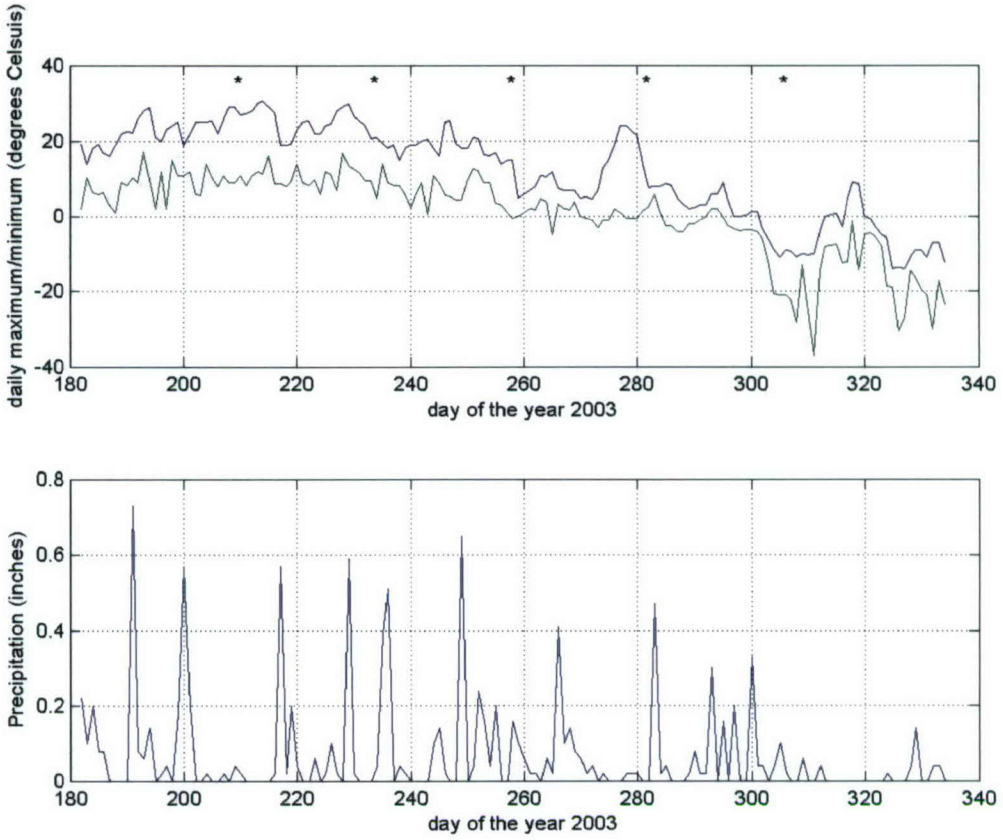

Figure 11: Daily temperature and precipitation from the airport closest to Key Lake Mine. The stars (*) in the upper plot denote the RADARSAT-1 acquisitions.

The baseline information and terrain elevation for a 2π change in phase is listed in Table 5 for all the combinations of passes that provided a reasonable coherence. The relatively large $\mathbf{B}_{VEL}$ is an indication that the platform trajectories were even more skewed than those of the Range Mine acquisitions. Considering the latitude of the platform, this is not too surprising. All the passes have a reasonable perpendicular baseline for interferometry.

For a more comprehensive analysis of change, we again consider both image magnitude and coherence. For an easier display of the change in the magnitudes, 2 RGB images were formed from the magnitudes of the five acquisitions. Figure 12 is the RGB image containing the magnitude images of 28 July (red), 21 August (green), and 14 September (blue). Figure 13 is the RGB image containing the magnitude image from 14 September (red), 8 October (green), and 1 November (blue). In both cases, the scene covers an area of approximately 77 km x 50 km.

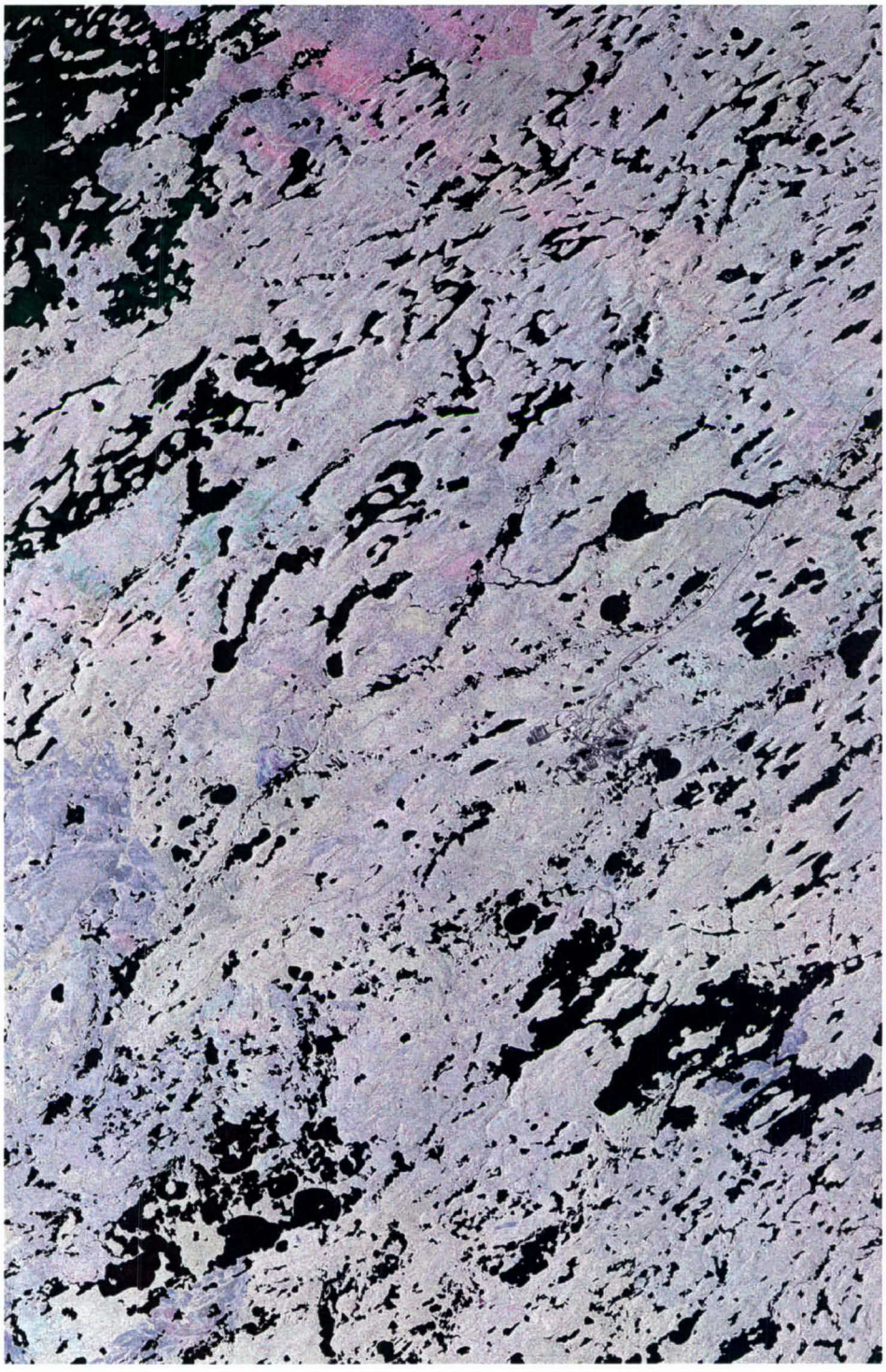

Figure 12: Magnitude image from 28 July 2003 (red), 21 August 2003 (green), and 14 September 2003 (blue) covering an area 77 km x 50 km.

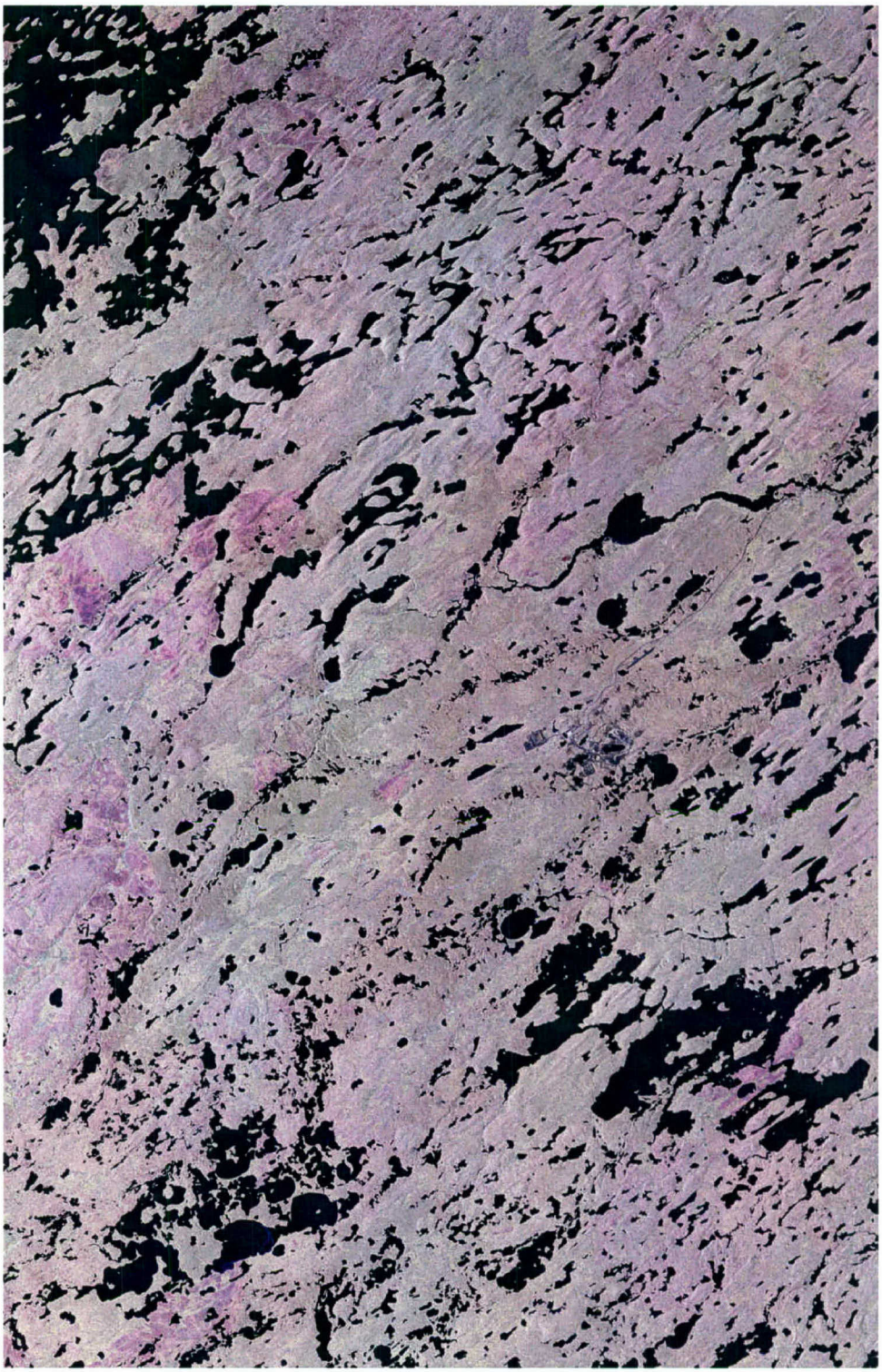

Figure 13: Magnitude image from 14 September 2003 (red), 8 October 2003 (green), and 1 November 2003 (blue) covering an area 77 km x 50 km.

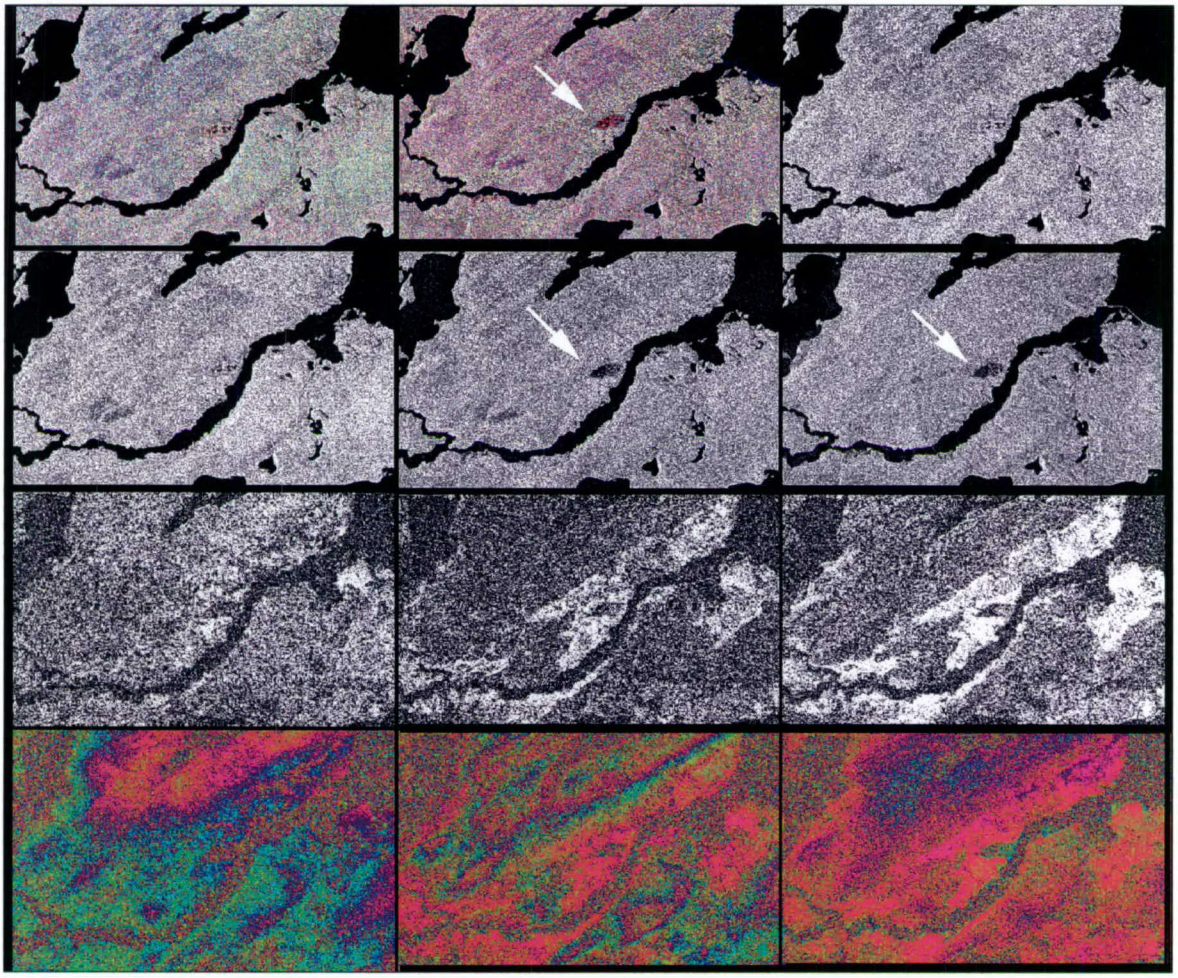

Figure 14: Detail from the Key Lake scene showing a saucer-shaped area of change. First row from the left are the RGB magnitude image with the July/August/September data set, the RGB magnitude image with the September/October/November 2003 data set, and the individual magnitude images from the August data set. The second row from the left are the individual magnitude images from the September, October, and November data sets. Third row from the left are the coherence images from the July/August, August/September, and September/October data sets respectively. Fourth row from the left are the corresponding ellipsoid corrected phase images.

The RGB images show several subtle and gradual colour changes. In view of the fairly constant rain that fell in the area, these changes may be the result of changes in ground moisture, and in turn indicates changes in terrain type. Scattering from bare soil is obviously affected the most by accumulation of ground moisture. By contrast, rocky terrain is affected the least by changes in ground moisture and should stand out as shades of grey. Scattering from trees and other areas of heavy vegetation may also change with time and appear differently in the magnitude images. They are also, however, subject to phase decorrelation and would show up as areas of low coherence.

Of interest are regions with clearly delineated colour changes in the RGB image. One such area appears in red, just above the river, just to the right and north of scene centre in Figure 13. Figure 14 shows the saucer-shaped site in more detail at scene centre. From the first two

images in the first row are the RGB images of the site corresponding to Figure 12 & Figure 13. Some of the individual B&W magnitude images appear in the next four frames. The last image in the first row is the 21 August acquisition. The second row from left to right are the magnitude images from the September 14, October 8, and November 1 acquisitions, respectively. Third row from the left are the coherence images from the July/August, August/September, and September/October datasets, respectively. Fourth row from the left are the corresponding ellipsoid corrected phase images. The saucer shaped anomaly is clearly visible in the October and November scenes. It is barely visible in the September scene, and completely absent in the August (and July) scenes. It appears very distinctly in the September/October coherence scene as a (black) region low coherence surrounded by (white) areas of high coherence. The lack of coherence is reflected in the phase image by phase noise. Being so close to the edge of the river it could be localised flooding, perhaps due to a temporary beaver dam.

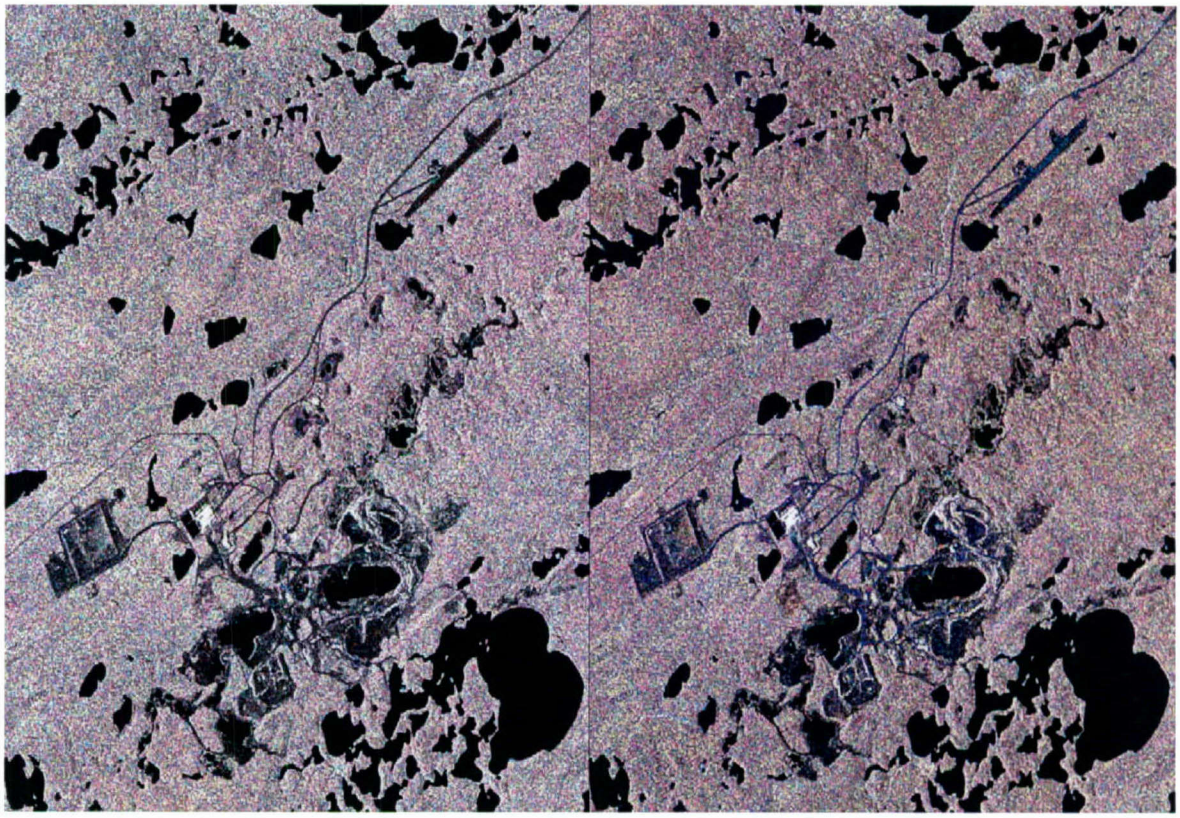

Figure 15 Detail from Figure 12 (left) and Figure 13 (right) over Key Lake Mine, covering an area 9.9 km x 9.5 km.

The mine is the dark region just to the right and south of the scene centre of Figure 12 & Figure 13. It is shown in full resolution in the corresponding RGB image of Figure 15. The (ellipsoid corrected) phase and coherence are shown in Figure 16 & Figure 17. In both cases the left image is the 21 August/28 July pair, the centre image is the 21 August/14 September, and the right image of is the 14 September/8 October pair. Speckle correlation tests show that ionospheric effects are minimal for these data sets. We are unable to make an assessment as to the presence, or strength of any tropospheric effects.

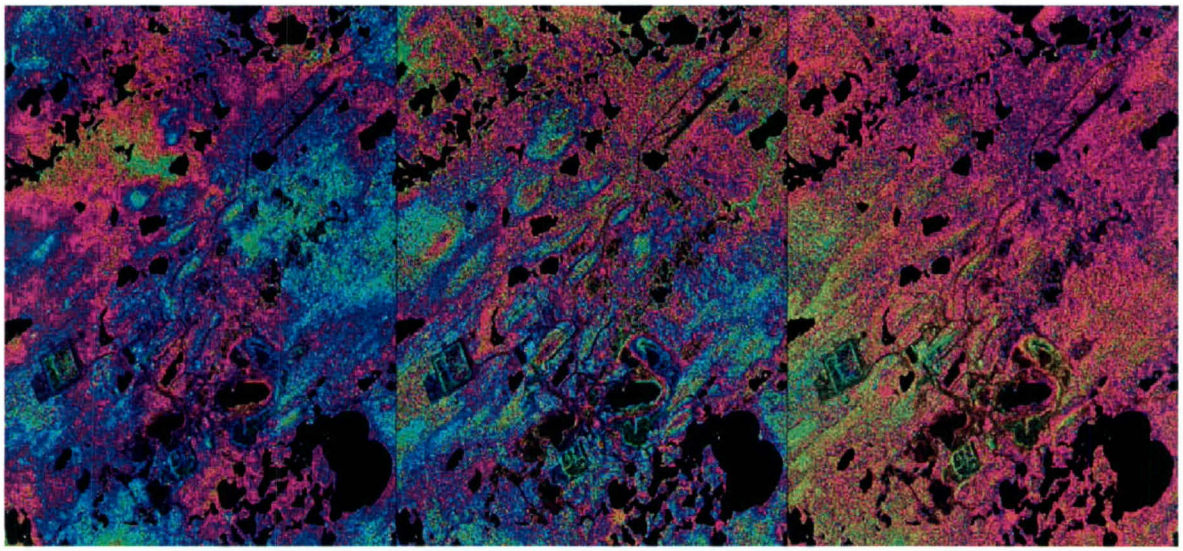

Figure 16: Ellipsoid corrected phase over Key Lake from 21August/28July (left), 21August/14September (centre) and 14Sepember/8October (right). The phase is wrapped between $-\pi$ and $+\pi$.

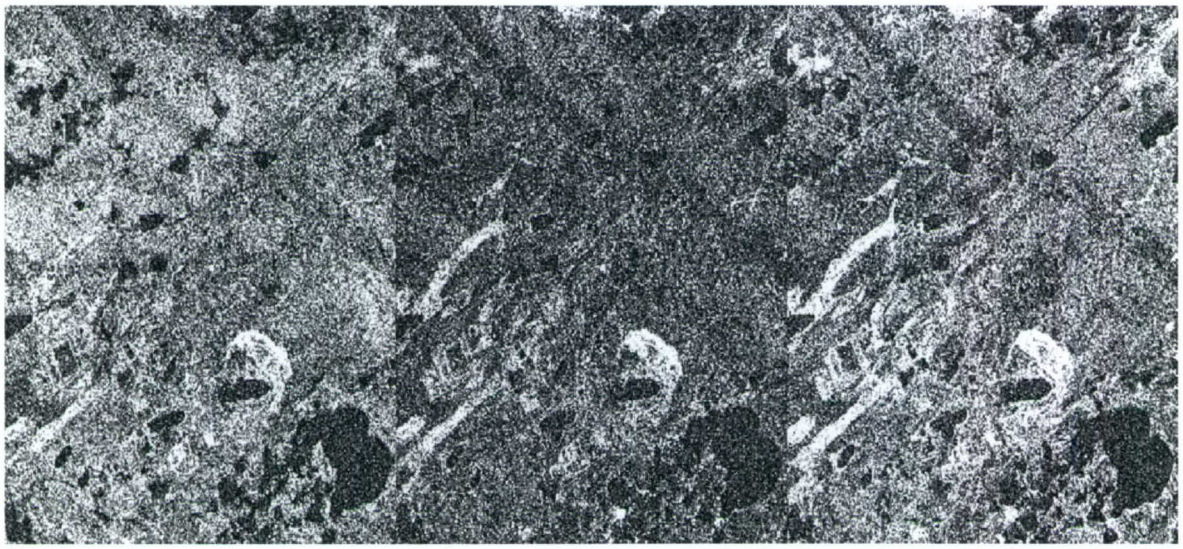

Figure 17: Coherence over Key Lake from 21August/28July (left), 21August/14September (centre) and 14September/8October (right). White signifies perfect coherence between the pair, black signifies complete decorrelation.

Of the three different types of images, the RGB images of the change in magnitudes are the easiest to work with. The coherence images are inherently much lower in resolution and (like the phase images) are quite noisy. Due to the lack of resolution, the coherence images are more useful in distinguishing larger regions of change than in details of the mine itself. Indeed they clearly demark stable (high coherence) and unstable (low coherence) regions, information that is not present in the magnitude images.

Examining the RGB images in Figure 15 in more detail, we observe a few areas of change. There are a few very small but distinct colour changes near the road network at centre of the mine. In the RGB image on the right in Figure 15, just left of the central mine area is an extended region with a distinct pinkish colour. In the coherence images, that same area is distinguished from its surroundings by its high coherence.

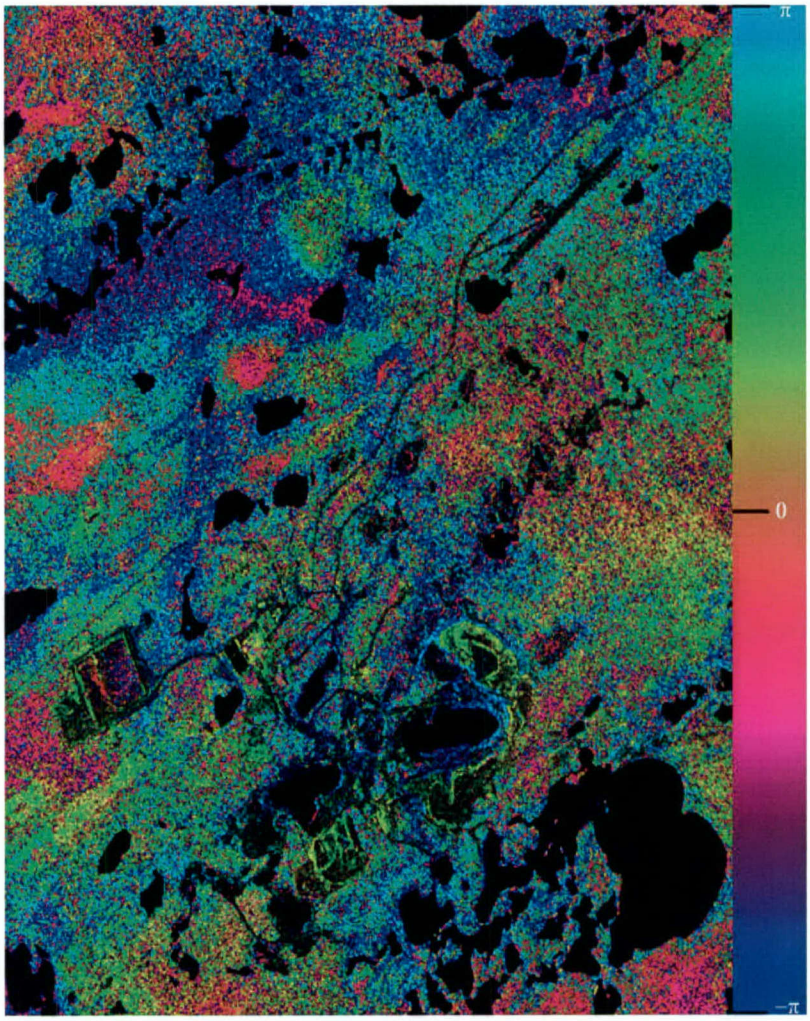

Figure 18: Estimation of terrain subsidence (in radians) between 21August/28July and 21August/14September data sets. Lack of ground control points and difficulties with phase unwrapping did not permit adequate baseline and phase calibration

It is difficult to make any assessment of change in the mine tailings or presence of any terrain subsidence from these magnitude, coherence, or raw phase images. Further processing of the data to terrain subsidence or height estimation is required. This procedure was outlined in the later part of Figure 1, and is the more complex portion of the processing. Once again, we lack sufficient information as to permit accurate deformation or terrain height estimation. We don't have sufficient information to assess the strength, or even the presence, of any tropospheric effects. We lack GCP or an accurate Digital Terrain Model to effect the baseline or phase calibration. Nevertheless, an estimation of the terrain subsidence was attempted

using (12). The Estimation of terrain subsidence (in radians) between 21 August/28 July and 21 August/14 September data sets appears in Figure 18. The colour deviations are more likely due to errors in baseline and phase calibration problems than terrain subsidence. But we can conclude that there was no terrain subsidence on the order of 10s of centimetres. These would have formed very characteristic rings in the deformation image, which are not visible in the image.

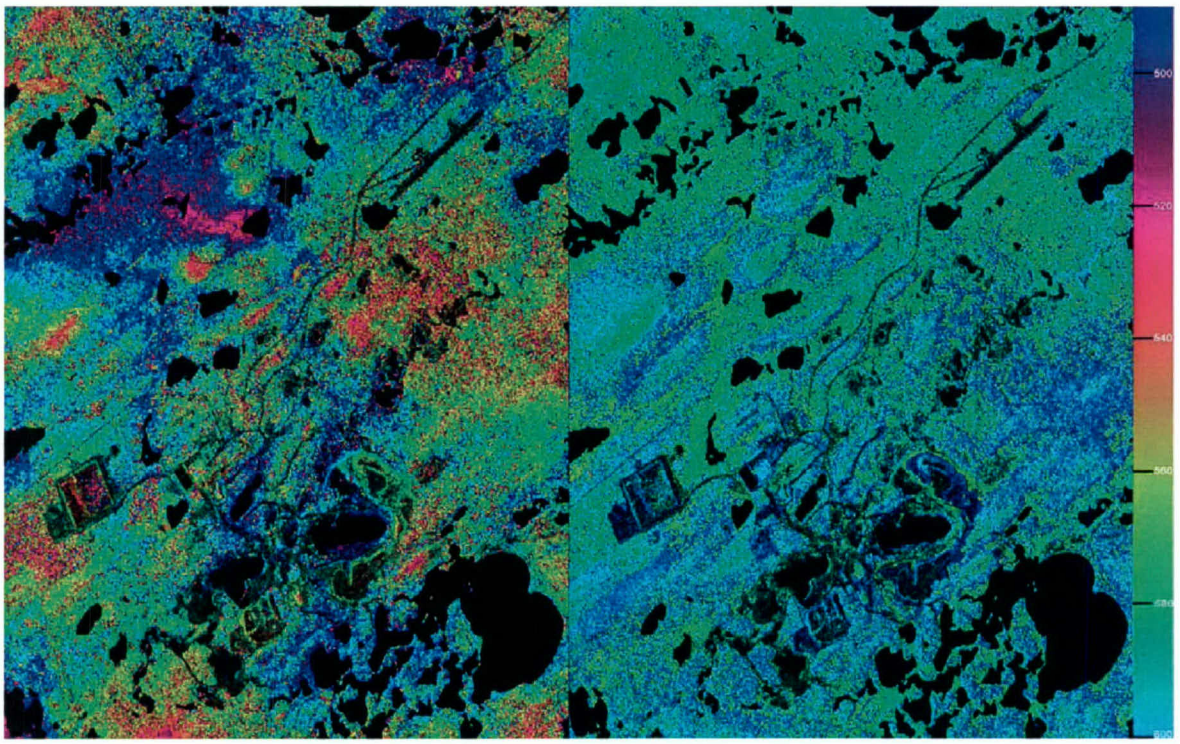

Figure 19: Estimation of terrain height(in meters) for (on the left) 21Aug/28Jul InSAR pair and (on the right) 21Aug/14Sep InSAR pair over Key Lake. Lack of ground control points and the consequent difficulties calibrating the baseline and phase, resulted in this obvious discrepancy in elevation between the two images.

An attempt at terrain height estimation, using (9) is shown in Figure 19. The figure on the left is the 21 August/28 July InSAR pair. The figure on the right is the 21 August/14 September InSAR pair. The two figures should be the same. Their difference is almost certainly due to baseline and phase errors. Of the available radar satellites, the orbit of RADARSAT-1 is known least accurately, and therefore subject to the greatest baseline, and consequently phase errors.

Summary and Conclusion

This report examined the potential of RADARSAT-1 satellite repeat-pass interferometry for change detection. Two sets of interferometric data were acquired, both over sites of active uranium mines. Over the first site, Range Mine located in South Australian, the data acquired included an interferometric quadruplet in the ascending mode, and an interferometric triplet in the descending mode. Over the second site, Key Lakes Mine in Saskatchewan, the data acquired included an interferometric quintuplet. Besides weather data and maps of the airport near both mines, no other ground truth was available.

Interferometric processing of the data to magnitude, coherence, and (earth-ellipsoid corrected) phase (potentially a fully automated task) proceeded normally. The image magnitudes as well as the coherence (a statistical measure of the phase noise) both provide valuable means of detecting scene changes. By assigning red, green and blue to three of the magnitude images and thereby creating an RGB image, even very subtle changes in image magnitudes are easily discernable. The RGB magnitude change images supplement the coherence image, and together offer a potentially valuable tool for wide area surveillance and long term monitoring. They potentially provide important contextual information in the immediate and extended area of the mine.

The coherence image, being a statistical measure of the phase noise, will always be lower in resolution than the 9 meters resolution of magnitude (or phase) images in single-look fine beam mode. The 3 meters resolution of RADARSAT-2, when it is launched at the end of 2005, will address this limitation. Its full polarimetric mode, and interferometric-polarimetric capability will also be of great value for change detection.

The three-colour RGB images over Range Mine proved to be a valuable tool for wide area surveillance. They showed large areas of flooding north of, and close to, the mine. Subtler colour changes pointed to possible ground saturation in large areas around the mine. In the mine complex itself, two areas with distinct colour changes are visible in the RGB images. These could be the result of man-induced changes to the ground (objects added or removed). Given the extensive flooding that affected the entire region, the change in the magnitudes could also be the result of increased terrain moisture. No doubt due to the flooding, the entire dataset lacked significant coherence. Therefore, no coherence information was possible.

The three-colour magnitude change images of the Key Lakes Mine region also showed interesting subtle terrain changes throughout the entire scene. A small but clearly delineated area of change visible near a river, just north of the mine is of particular interest. Visible within the mine complex itself there are regions of subtle colour change. Coherence, in general, was fair. Distinct regions of high and low coherence appear within the mine complex. However, due to the lack of resolution, interpretation of the change is difficult.

Accurate estimation of the terrain subsidence and terrain height from the (earth-ellipsoid corrected) phase of RADARSAT-1 is a much more difficult and cumbersome procedure. In the two cases considered here, accurate estimation of the terrain subsidence and terrain height were not possible. The limited resolution of the system did not permit pixel averaging which

would have reduced the phase noise and simplified phase unwrapping. The lack of sufficient ground truth did not permit accurate baseline and phase calibration. Speckle correlation tests ascertained that no significant ionospheric artefacts were present in any of datasets acquired. However, no assessment could be made in regards to the strength (or even presence) of tropospheric phase errors. As a consequence, the terrain height could not be used to detect any changes in height of the mine tailings. Subtle millimetre or centimetre terrain subsidence was also undetectable. But with analysis of the phase, we could conclude that (coherent) terrain subsidence of the order of 10s of centimetres or more were not present. These would have left clearly distinguishable and very characteristic ring-loke patterns in the phase subsidence image.

References

1. P.A. Rosen, S.Hensley, I.R. Joughin, F.K. Li, S.N. Madsen, E. Rodriguez and R.M. Goldstein, "Synthetic Aperture Radar Interferometry," *Proc. IEEE*, vol. 88, no. 3, pp.332-381, March 2000.

2. M. Santoro *et al.*, " Monitoring Urban Areas by Means of Coherence Levels", *ESA FRINGE '99 Conference Proceedings* (see http://www.esa.int/fringe99, last accessed May 2004), 1999.

3. R. Bamler and P. Hartl, "Synthetic Aperture Radar Interferometry," *Inverse Problems*, vol. 14, 1998, pp. R1-R54.

4. K.E. Mattar, L. Gallop, J. Lang, "Alert 2002 ground truth missions for Arctic shoreline delineation and feature extraction," (DRDC Ottawa TM 2002-147), Defence R&D Canada – Ottawa, 2002.

5. F. Bénédicte, D. Christophe, and A. José, "Observation and modeling of the Saint-Etienne-de Tineé landslide using SAR interferometry," *ESA FRINGE'96 Conference Proceedings* (see http://www.geo.unizh.ch/rsl/fringe96, last accessed November 2004), 1996.

6. C. Carnec and C. Delacourt, "Three years of mining subsidence monitored by SAR interferometry, near Gardanne, France," *ESA FRINGE'99 Conference Proceedings* (see http://www.esa.int/fringe99, last accessed May 2004), 1999.

7. R. Touzi, A. Lopes, J. Bruniquel and P.W. Vachon, "Coherence Estimation for SAR Imagery," *IEEE Transactions on Geoscience and Remote Sensing*, vol. 37, no. 1, pp. 135-149, January 1999.

8. J.M. Rignot and J.J. van Zyl, "Change detection techniques for ERS-1 SAR data," *IEEE Transactions on Geoscience and Remote Sensing*, vol. 31, pp. 896-906, July 1993.

9. H.A. Zebker and H. Villasenor, "Decorrelation in Interferometric Radar Echoes," *IEEE Transactions on Geoscience and Remote Sensing*, vol. 30, no. 5, pp. 950-959. September 1992.

10. F. Gatelli, A. M. Guarnieri, F. Parizzi, P. Pasquali, C. Pratti and F. Rocca, "The Wavenumber Shift in SAR Interferometry," *IEEE Transactions on Geoscience and Remote Sensing,* vol. 32, no. 4, pp. 855-865, July 1994.

11. K.E. Mattar, A.L. Gray, D. Geudtner, and P.W. Vachon, "Interferometry for DEM and Terrain Displacement: Effects of Inhomogeneous Propagation," *Canadian Journal of Remote Sensing*, vol. 25, no. 1, pp. 60-69, March 1999.

12. R. Scheiber and A. Moriera, "Coregistration of Interferometric SAR Images Using Spectral Diversity," *IEEE Transactions on Geoscience and Remote Sensing*, vol. 38, no. 5, pp. 2179-2190, September 2000.

13. J.J. Mohr and S.N. Madsen, "Geometric Calibration of ERS Satellite SAR Images", *IEEE Transactions on Geoscience and Remote Sensing*, vol. 39, no., 4, pp. 842-840, April 2001.

14. F.-H. Massmann, J. C. Neumayer, K. Raimondo, K. Enninghorst, and H. Li, "Quality of the D-PAF orbits before and after the inclusion of PRARE data," in *Proc. 3rd ERS Symp.: Space at the Service of our Environment*, Vol. 3, Florence, Italy, pp. 1655–1660, March 1997.

15. H. Rufenacht, R.J. Proulx and P.J. Cefola, "Improvement of RADARSAT Image localization," *The international symposium on Geomatics in the Era of RADARSAT (GER '97)*, Ottawa, Canada, May 25-30, 1997.

16. H. Tarayre-Oriot and D. Massonnet, "Atmospheric artifacts on interferomgrams," *ESA FRINGE'96 Conference Proceedings* (see http://www.geo.unizh.ch/rsl/fringe96/) 1996.

17. Personal communication from Bob Truong, 2003.

List of symbols/abbreviations/acronyms/initialisms

CNSC	Canadian Nuclear Safety Commission
CSA	Canadian Space Agency
DEM	Digital Elevation Model
DND	Department of National Defence
DRDC	Defence Research & Development Canada
ERS	European Remote Sensing
ESA	European Space Agency
GCP	Ground Control Point
InSAR	Interferometric SAR
PRF	Pulse Repetition Frequency
SAR	Synthetic Aperture Radar
SLC	Single look complex
SRI	Satellite radar interferometry

DOCUMENT CONTROL DATA

(Security classification of title, body of abstract and indexing annotation must be entered when the overall document is classified)

1. ORIGINATOR (the name and address of the organization preparing the document. Organizations for whom the document was prepared, e.g. Establishment sponsoring a contractor's report, or tasking agency, are entered in section 8.)

   Defence R&D Canadata – Ottawa
   Department of National Defence
   Ottawa, Ontario, Canada K1A 0K2

2. SECURITY CLASSIFICATION (overall security classification of the document, including special warning terms if applicable)

   UNCLASSIFIED

3. TITLE (the complete document title as indicated on the title page. Its classification should be indicated by the appropriate abbreviation (S,C or U) in parentheses after the title.)

   Change detection using RADARSAT-1 interferometry: mine site monitoring (U)

4. AUTHORS (Last name, first name, middle initial)

   Mattar, Karim E.

5. DATE OF PUBLICATION (month and year of publication of document)

   December 2004

6a. NO. OF PAGES (total containing information. Include Annexes, Appendices, etc.)

   46

6b. NO. OF REFS (total cited in document)

   17

7. DESCRIPTIVE NOTES (the category of the document, e.g. technical report, technical note or memorandum. If appropriate, enter the type of report, e.g. interim, progress, summary, annual or final. Give the inclusive dates when a specific reporting period is covered.)

   Technical Memorandum

8. SPONSORING ACTIVITY (the name of the department project office or laboratory sponsoring the research and development. Include the address.)

   DRDC Ottawa TM 2004-261

9a. PROJECT OR GRANT NO. (if appropriate, the applicable research and development project or grant number under which the document was written. Please specify whether project or grant)

   15eu23

9b. CONTRACT NO. (if appropriate, the applicable number under which the document was written)

10a. ORIGINATOR'S DOCUMENT NUMBER (the official document number by which the document is identified by the originating activity. This number must be unique to this document.)

10b. OTHER DOCUMENT NOS. (Any other numbers which may be assigned this document either by the originator or by the sponsor)

11. DOCUMENT AVAILABILITY (any limitations on further dissemination of the document, other than those imposed by security classification)

- (x) Unlimited distribution
- ( ) Distribution limited to defence departments and defence contractors; further distribution only as approved
- ( ) Distribution limited to defence departments and Canadian defence contractors; further distribution only as approved
- ( ) Distribution limited to government departments and agencies; further distribution only as approved
- ( ) Distribution limited to defence departments; further distribution only as approved
- ( ) Other (please specify):

12. DOCUMENT ANNOUNCEMENT (any limitation to the bibliographic announcement of this document. This will normally correspond to the Document Availability (11). However, where further distribution (beyond the audience specified in 11) is possible, a wider announcement audience may be selected.)

13. ABSTRACT (a brief and factual summary of the document. It may also appear elsewhere in the body of the document itself. It is highly desirable that the abstract of classified documents be unclassified. Each paragraph of the abstract shall begin with an indication of the security classification of the information in the paragraph (unless the document itself is unclassified) represented as (S), (C), or (U). It is not necessary to include here abstracts in both official languages unless the text is bilingual).

This study examines the potential of using satellite repeat-pass interferometry for wide-area surveillance and change detection. Several RADARSAT-1 interferometric datasets were acquired in 2003 over active mines in South Australia and Saskatchewan, Canada. Three-colour RGB images derived from the various image magnitudes supplements and complements the interferometric coherence information for detecting even subtle scene changes. Together they were found to be a potentially valuable tool for wide area surveillance and long term site monitoring, providing potentially important contextual information. The limited resolution of RADARSAT-1 did not permit conclusive assessment of changes detectable in the mine complex itself, and the lack of ground truth did not permit accurate terrain height estimation. The absence of ring-like phase patterns that characterize decimetre-level terrain subsidence implies that terrain subsidence was not present within the scene.

14. KEYWORDS, DESCRIPTORS or IDENTIFIERS (technically meaningful terms or short phrases that characterize a document and could be helpful in cataloguing the document. They should be selected so that no security classification is required. Identifiers such as equipment model designation, trade name, military project code name, geographic location may also be included. If possible keywords should be selected from a published thesaurus. e.g. Thesaurus of Engineering and Scientific Terms (TEST) and that thesaurus-identified. If it is not possible to select indexing terms which are Unclassified, the classification of each should be indicated as with the title.)

Interferometric SAR
Coherence
Synthetic Aperture Radar
Change Detection

Defence R&D Canada

Canada's leader in defence
and national security R&D

R & D pour la défense Canada

Chef de file au Canada en R & D
pour la défense et la sécurité nationale

www.drdc-rddc.gc.ca